FULL PAPER

Dalton
www.rsc.org/dalton

Monometallic lanthanide complexes with tridentate 2,6-dicarboxamidopyridine ligands. Influence of peripheral substitutions on steric congestion and antenna effect †

Thierry Le Borgne,[a] Jean-Marc Bénech,[a] Sébastien Floquet,[a] Gérald Bernardinelli,[b] Christian Aliprandini,[a] Philippe Bettens[a] and Claude Piguet*[a]

[a] *Department of Inorganic, Analytical and Applied Chemistry, University of Geneva, 30 quai E. Ansermet, CH-1211 Geneva 4, Switzerland. E-mail: Claude.Piguet@chiam.unige.ch*

[b] *Laboratory of X-ray Crystallography, 24 quai E. Ansermet, CH-1211 Geneva 4, Switzerland*

Received 30th June 2003, Accepted 26th August 2003
First published as an Advance Article on the web 8th September 2003

The systematic investigation of steric and electronic effects on the formation of lanthanide complexes with the tridentate *N*,*N*,*N*′,*N*′-tetraalkylpyridine-2,6-dicarboxamide *ONO* ligands (alkyl = ethyl: **L5**, isopropyl: **L6** and benzyl: **L7**) shows a reduced affinity with increasing steric demand in the order **L5** < **L6** < **L7**. $[Ln(\mathbf{L}i)]^{3+}$ and $[Ln(\mathbf{L}i)_2]^{3+}$ are formed with the three ligands, but 1 : 3 complexes are strictly limited to $[Ln(\mathbf{L5})_3]^{3+}$ and $[Ln(\mathbf{L6})_3]^{3+}$ because of the significant steric congestion provided by the twelve benzyl groups located along the three-fold axis in $[Ln(\mathbf{L7})_3]^{3+}$. Comparisons between **L6** and **L7** in the 1 : 2 complexes evidence superimposable pseudo-monocapped square antiprismatic coordination spheres in the crystal structures of $[Ln(\mathbf{L}i)_2(H_2O)_2(CF_3SO_3)](CF_3SO_3)_2$ (i = 6, Ln = Eu: **9**; i = 7, Ln = Gd: **10**). Photophysical properties of $[Ln(\mathbf{L6})_2]^{3+}$ and $[Ln(\mathbf{L7})_2]^{3+}$ (Ln = Eu, Gd, Tb, Lu) are similar except for improved quantum yields for $[Ln(\mathbf{L7})_2]^{3+}$ (Ln = Eu, Tb) which can be assigned to a slightly more efficient **L7** ⟶ Ln^{III} energy transfer process. The removal of two benzyl groups in the analogous *N*,*N*′-dibenzylpyridine-2,6-dicarboxamide ligand (**L8**) restores the formation of stable triple-helical complexes as demonstrated by the crystal structure of $[Tb(\mathbf{L8})_3]_2(CF_3SO_3)_6$ (**11**). However, the existence of intricate mixtures of isomers in solution which are blocked on the NMR time scale limits their use as building blocks for the design of polymetallic d–f and f–f helicates.

Introduction

Since the 4f valence shells of the trivalent lanthanides, Ln^{III}, are shielded from external perturbations by the filled $5s^2$ and $5p^6$ orbitals, the interaction of the metallic core with the surrounding ligands in coordination complexes is mainly electrostatic.[1] Minor, but predictable tuning of the electronic, optical and magnetic properties can be then traced back to weak crystal-field effects induced by the donor atoms in the first coordination sphere.[2] The use of ligand design for the optimization of one particular property in the final lanthanide complexes is thus attractive, but it remains challenging because (i) the structural control of the coordination sphere mainly relies on weak interstrand interactions,[3] (ii) polarization effects strongly affect crystal-field parameters,[4] and (iii) the entropic contribution to the complexation process is considerable which complicates theoretical modeling.[5] In this context, semi-rigid tridentate binding units derived from 2,2′:6′,2″-terpyridine (**L1**) are valuable candidates because saturated nine-coordinate monometallic lanthanide complexes requires the helical wrapping of only three ligands in $[Ln(\mathbf{L1})_3]^{3+}$ which minimizes the entropic cost.[6,7] Moreover, non-covalent interstrand interactions controlling the size and geometry of the metallic site can be programmed *via* peripheral modifications of **L1**, thus leading to tuneable thermodynamic,[8] structural[9] and optical[10] properties. However, the limited enthalpic stabilization of $[Ln(\mathbf{L1})_3]^{3+}$ is a severe handicap for the design of efficient complexes for aqueous An^{III}/Ln^{III} separations (nuclear waste management),[5b] and for the development of functional luminescent probes.[6–10] This drawback can be partially overcome thanks to the replacement of the distal pyridine rings in **L1** with more polarizable dialkyltriazinyl rings in **L2** which significantly improves the affinity for Ln^{III}.[11–13] The alternative connection of distal five-membered heterocycles in **L3**[14] and **L4**[15] provides an optimal fit between the tridentate cavity and the size of Ln^{III}, and remarkable size-discriminating effects along the lanthanide series have been evidenced for $[Ln(\mathbf{L4})_3]^{3+}$. On the other hand, efficient energy back-transfers in $[Tb(\mathbf{L4})_3]^{3+}$ [15c] and quenching processes involving low-lying LMCT states in $[Eu(\mathbf{L4})_3]^{3+}$ [16] prevent their use as luminescent building blocks in sophisticated polymetallic triple-stranded d–f and f–f helicates.[3,6] The introduction of aromatic substituents in **L4** (R = benzoic esters or benzyl alcohols)[17] does not significantly improve the antenna effect, but the long distance separating the metal from the chromophoric groups may explain this failure, as recently demonstrated in rigid C_4-symmetrical macrocyclic lanthanide platforms grafted with peripheral aromatic groups.[18] In order (i) to put the light-harvesting chromophores closer to the metal ion in triple-helical lanthanide complexes and (ii) to develop a novel library of tridentate receptors for the selective complexation and sensitization of lanthanides, we have resorted to *N*,*N*,*N*′,*N*′-tetraalkylpyridine-2,6-dicarboxamide *ONO* ligands derived from **L5** for which stable and moderately luminescent (Ln = Eu, Tb) triple-helical complexes $[Ln(\mathbf{L5})_3]^{3+}$ have been reported.[19] A thorough investigation of the solution and solid state structures of $[Ln(\mathbf{L5})_3]^{3+}$ demonstrated that the OC–N(amide) bonds display considerable double-bond character which arranges the alkyl residues R^1 close to the three-fold axis and the metal ion.[19] In this contribution, we report on the steric and electronic consequences brought by the connection of bulky semi-flexible benzyl chromophores to the terminal carboxamide side arms in **L7**. Particular attention is focused on the thermodynamic, structural and photophysical properties in the resulting lanthanide complexes $[Ln(\mathbf{L7})_n]^{3+}$ (n = 1–3) which are

† Electronic supplementary information (ESI) available: tables of NMR data (Table S1), elemental analyses (Table S2), calculated distribution of isomers for $[Ln(\mathbf{L8})_3]^{3+}$ (Table S3) structural data for the lanthanide coordination sphere (Table S4) and intra- and intermolecular stacking interactions (Table S5) in $[Tb(\mathbf{L8})_3]_2(CF_3SO_3)_6$, and crystallographic data (Table S6). Figures showing steroviews of **L8** (Fig. S1) and $[Tb(\mathbf{L8})_3]_2(CF_3SO_3)_6$ (Fig. S7), spectrophotometric titration of **L7** (Fig. S2), solution structures of $[Ln(\mathbf{L6})_2]^{3+}$ and $[Ln(\mathbf{L7})_2]^{3+}$ (Fig. S3), the coordination sphere in $[Gd(\mathbf{L7})_2(H_2O)_2(CF_3SO_3)]^{2+}$ (Fig. S4), distribution curves (Fig. S7); emission spectra (Fig. S6) and partial superimposition of both molecules of the asymmetric unit in **11** (Fig. S8). See http://www.rsc.org/suppdata/dt/b3/b307413g/

DOI: 10.1039/b307413g

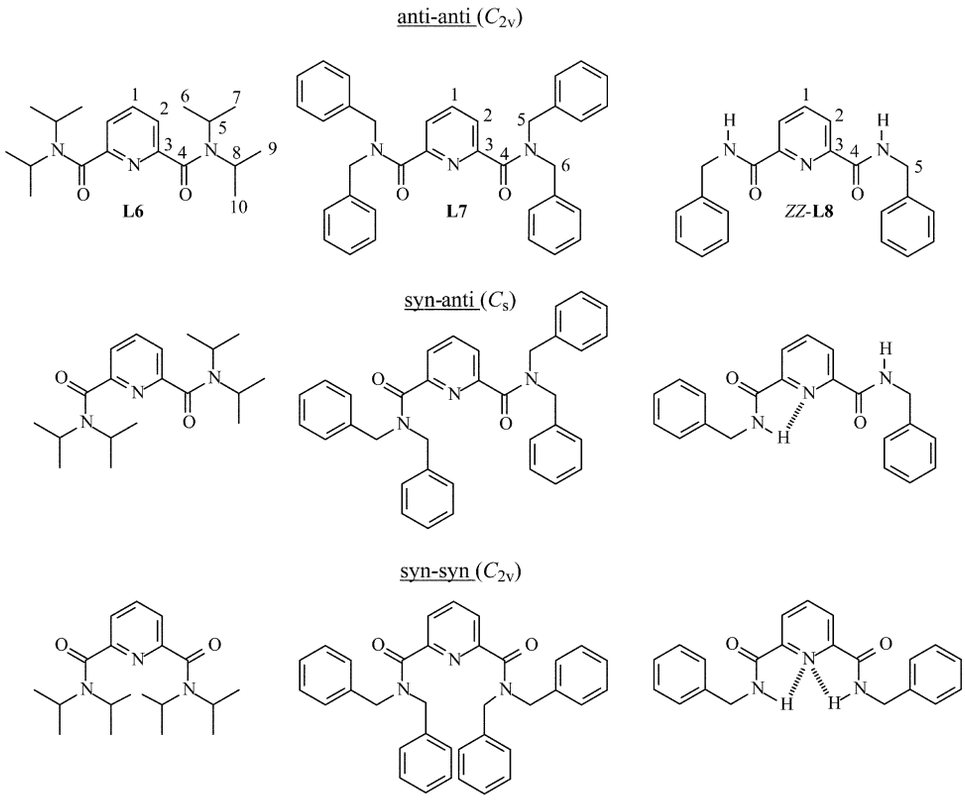

Fig. 1 Numbering of the carbon atoms for NMR measurements and possible conformations of the free ligands **L6**, **L7** and **L8**.

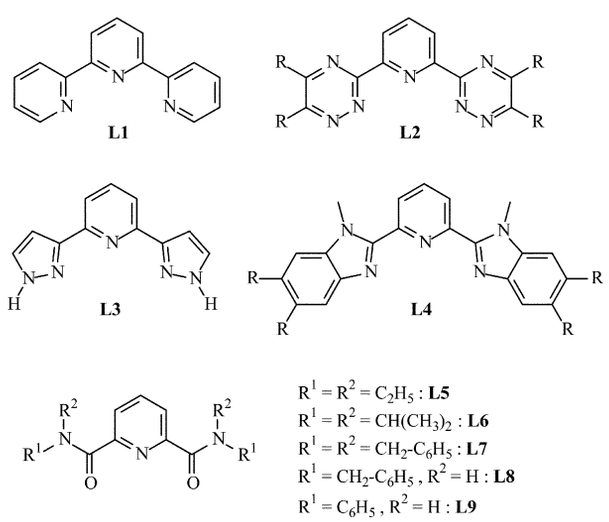

Scheme 1

compared with those provided by **L6** (similar steric constraints with no peripheral chromophoric unit) and **L8** (similar benzyl chromophores with reduced steric congestions).

Results and discussion

Syntheses and structures of the ligands L6–L8

The tridentate ligands **L6**–**L8** are obtained in 80–82% yields *via* the amidation of 2,6-pyridinedicarboxylic acyl chloride with an excess of the corresponding amine. Room-temperature ^{1}H NMR spectra reflect C_{2v}-symmetrical geometries characterized by (i) two equivalent carboxamide side arms and (ii) enantiotopic methyl groups in **L6** (H6–H7 and H9–H10), or methylene protons in **L7** (H5–H5′ and H6–H6′) and in **L8** (H5–H5′, Fig. 1, Table S1 ESI†). The rotations about the OC–N amide bonds are blocked on the NMR time scale as demonstrated by non-equivalent isopropyl groups in **L6** and benzyl groups in **L7**. Variable-temperature data (293–433 K, d^6-DMSO) show the coalescence of the signals of the methyl groups (H6–H7 with H9–H10) at T_c = 353 K for **L6,** and that of the methylene protons (H5–H5′ with H6–H6′) at T_c = 363 K for **L7**. Calculations using the Eyring model (eqns. (1)–(3))[20]

$$\Delta G^{\neq} = RT \ln\left(\frac{k_B T}{kh}\right) \quad (1)$$

$$k = \frac{\pi \delta \nu}{X} \quad (2)$$

$$X^6 - 6X^4 + [12 - 27(\Delta p)^2]X^2 - 8 = 0 \quad (3)$$

give $\Delta G^{\neq}$(**L6**) = 71(3) kJ mol^{-1} and $\Delta G^{\neq}$(**L7**) = 74(3) kJ mol^{-1} at the coalescence temperatures (k is the rate constant at T_c, $\delta\nu$ is the chemical shift difference in absence of exchange taken from the ^{1}H NMR data at 293 K, R, k_B and h are, respectively, the molar gas constant, the Boltzmann and Planck constants, Δp is the difference in population between the two exchangeable sites, and X is the solution of the polynomial expression given in eqn. (3) ($X = \sqrt{2}$ for $\Delta p = 0$ in this case)).[20] These activation energies are slightly smaller than those found for *N*,*N*′-dimethyformamide ($\Delta G^{\neq}$ = 86 kJ mol^{-1})[21] which reflects the increased delocalization of the electronic π density of the OC–N bond onto the electro-withdrawing pyridine ring in **L6** and **L7**.

The C_{2v} symmetry found for **L6** and **L7** is compatible with both the *anti-anti* or *syn-syn* conformations of the carboxamide side arms (or a fast exchange between these conformers, Fig. 1). However, the lack of NOE effects between the protons of the distal isopropyl (**L6**) or benzyl (**L7**) groups, and the pyridine H1 and H2 protons eventually establishes *syn-syn* conformations which minimize the repulsion between the dipole moments of the central pyridine ring and the connected carbonyl groups.

Table 1 Cumulative stability constants ($\log(\beta_{1n}^{Ln})$) for the complexes $[Ln(\mathbf{Li})_n]^{3+}$ (i = 5–7, n = 1–3, acetonitrile, 293 K)

		L5			L6			L7	
Metal	R^{Ln}/Å [a]	$\log(\beta_{11})$ [b]	$\log(\beta_{12})$ [b]	$\log(\beta_{13})$ [b]	$\log(\beta_{11})$	$\log(\beta_{12})$	$\log(\beta_{13})$	$\log(\beta_{11})$	$\log(\beta_{12})$
La(III)	1.216	7.4(3)	14.8(3)	21.0(3)	7.8(5)	14.0(7)	18.0(8)	5.4(5)	11.1(6)
Ce(III)	1.196	7.6(3)	14.3(4)	22.0(3)	7.4(4)	13.0(6)	17.9(7)		
Pr(III)	1.179	7.6(3)	14.6(3)	22.2(3)	8.0(6)	13.8(8)	17.5(9)		
Nd(III)	1.163	7.5(3)	13.8(4)	21.5(4)	7.7(5)	13.5(7)	17.5(8)		
Sm(III)	1.132	7.3(3)	14.4(4)	22.0(4)	8.5(6)	12.9(7)	18.4(8)		
Eu(III)	1.120	8.3(3)	15.3(3)	22.3(3)	8.3(6)	13.9(6)	17.6(7)	4.9(5)	9.8(6)
Gd(III)	1.107	7.9(3)	14.7(4)	22.6(4)	7.9(7)	13.7(9)	17.5(9)		
Tb(III)	1.095	8.2(3)	14.5(4)	22.9(4)	7.6(6)	13.8(7)	18.5(7)		
Dy(III)	1.083	7.5(3)	14.8(4)	22.5(4)	7.7(5)	14.4(6)	17.3(8)		
Ho(III)	1.072	7.3(4)	14.8(4)	22.3(4)	8.3(6)	14.2(7)	17.9(9)		
Er(III)	1.062	7.7(4)	14.4(4)	22.7(4)	8.3(5)	13.9(6)	17.5(8)		
Tm(III)	1.052	8.5(3)	16.0(3)	22.1(4)	7.9(6)	13.8(7)	17.8(9)		
Yb(III)	1.042	8.5(3)	15.6(3)	22.8(4)	7.7(4)	13.7(5)	16.7(6)		
Lu(III)	1.032	8.1(3)	15.2(3)	22.9(3)	7.6(4)	13.5(5)	17.3(6)	5.3(5)	9.7(6)
Y(III)	1.075	7.6(3)	14.6(4)	22.4(4)				4.9(5)	9.4(6)

[a] Ionic radii for nine-coordinate Ln^{III}.[29] [b] Taken from ref. 19.

Surprisingly, **L8** also exists as a single conformer with C_{2v}-symmetry although we expect a mixture of *EE*, *EZ* and *ZZ* isomers resulting from the blocked rotation about OC–N bonds in secondary amides (the *E* and *Z* notation refers to the the OC–N bond considered as a double bond). However, the formation of two intramolecular NH ··· N(pyridine) hydrogen bonds producing two fused five-membered rings in the *syn-syn* conformation strongly stabilizes the *ZZ* isomer according to *Etter*'s rules,[22] and **L8** consequently adopts a blocked *syn-syn-ZZ* conformation (Fig. 1). Variable-temperature ^{1}H NMR data do not affect the signals of the H5–H5′ protons in **L8** which suggests that $\Delta G^{\neq}$(**L8**) ⩾ $\Delta G^{\neq}$(**L6**) ≈ $\Delta G^{\neq}$(**L7**) for the rotation about the OC–N bonds.

The molecular structure of **L8** in the solid state confirms the exclusive formation of the *syn-syn-ZZ* isomer (Fig. 2) as previously reported for the analogous ligand **L9** in which the terminal benzyl groups are replaced with phenyl groups (Scheme 1).[23] The bonds lengths and bond angles are standard,[24] and two short contact interactions N3H03 ··· N1 = 2.32 Å and N2H02 ··· N1 = 2.36 Å suggest the existence of two strong intramolecular hydrogen bonds which are optimized by the almost coplanar arrangements of the carboxamide side arms (C1–C6–O1–N2 and C5–C14–O2–N3) with the central pyridine ring (interplanar angles 6.03(8) and 12.53(9)°; a similar structural pattern has been reported for **L9** with NH ··· N = 2.33–2.38 Å and average interplanar angle 24°).[23] For **L8**, each NH donor is further involved in one intermolecular hydrogen bond with the oxygen atom O2′ of a neighbouring ligand (x, ½ − y, ½ + z; N2H02 ··· O2′ = 2.22(3) Å, N2–H02 ··· O2′ = 154(2)° and N3H03 ··· O2′ = 2.26(3) Å, N3–H03 ··· O2′ = 165(2)°), thus forming chains approximately along the [001] direction. These chains are further packed through weak intermolecular offset face-to-face aromatic stacking interactions involving pyridine–pyridine pairs through a centre of inversion (separation 3.43 Å), and pyridine–benzyl pairs through a glide plane (separation 3.66 Å, interplane angle = 10.5°, Fig. S1, ESI†). We can thus safely assign the larger activation barrier for the rotation about the OC–N bonds observed for **L8** in solution to specific intramolecular NH ··· H hydrogen bonds which (i) stabilize the *ZZ* isomer and (ii) have no counterparts in **L6** and **L7**.

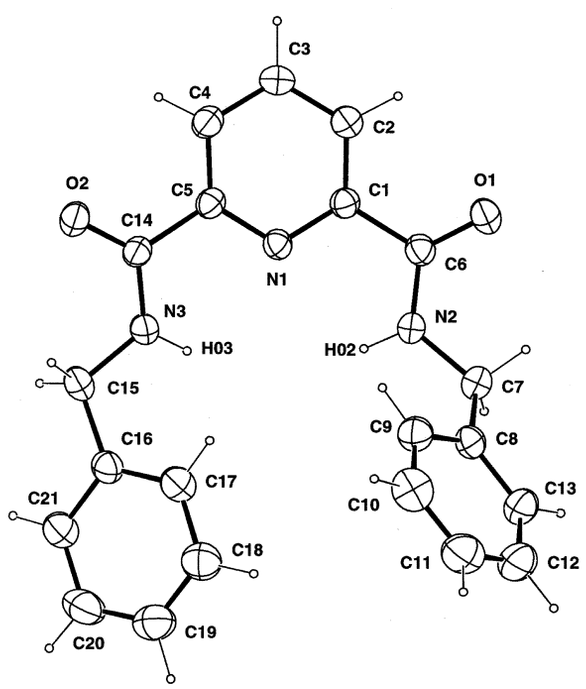

Fig. 2 ORTEP view of the ligand **L8** with atomic numbering scheme. Ellipsoids are represented at 40% probability level.

Stoichiometry, stability and dynamic of the complexes formed in solution between L6, L7 and trivalent lanthanides (Ln = La–Lu)

As previously reported for **L5**,[19] the absorption spectra of **L6** and **L7** are significantly modified both in shape and intensities upon complexation to Ln^{III}, and this allows a quantitative analysis of the complexation process by using spectrophotometric titrations (Fig. S2, ESI†). Titrations of **L6** (10^{-4} mol dm^{-3}) with $Ln(CF_3SO_3)\cdot xH_2O$ (Ln = La–Lu, x = 2–4; Ln : **L6** = 0.1–2.0) in acetonitrile show a smooth evolution of the absorption spectra with two marked end points for Ln : **L6** = 0.5 and Ln : **L6** = 1.0. Factor analysis[25] systematically confirms the formation of four absorping species assigned to **L6** and $[Ln(\mathbf{L6})_n]^{3+}$ (n = 1–3) as previously established for **L5**.[19] The spectrophotometric data can be satisfyingly fitted with non-linear least-squares techniques[26] to equilibria (4)–(6), and the associated formation constants are collected in Table 1.

$$Ln^{3+} + \mathbf{Li} \rightleftarrows [Ln(\mathbf{Li})]^{3+}: \log(\beta_{11}^{Ln}) \quad (4)$$

$$Ln^{3+} + 2\,\mathbf{Li} \rightleftarrows [Ln(\mathbf{Li})_2]^{3+}: \log(\beta_{12}^{Ln}) \quad (5)$$

$$Ln^{3+} + 3\,\mathbf{Li} \rightleftarrows [Ln(\mathbf{Li})_3]^{3+}: \log(\beta_{13}^{Ln}) \quad (6)$$

β_{11}^{Ln} and β_{12}^{Ln} for **L5** and **L6** are comparable within experimental errors and display the expected electrostatic trend (*i.e.* a slight increase of $\log(\beta_{11}^{Ln})$ with the decreasing size of the metal ion)[5a] resulting from the contraction of the ionic radii along the

lanthanide series (Fig. 3(a) and (b)). This points to similar affinities of the tridentate binding units for Ln^{III}, but the reduction of β_{13}^{Ln} by 3–4 orders of magnitude when going from **L5** to **L6** testifies to the increased steric constraints produced by the wrapping of three bulky tridentate strands in $[Ln(\mathbf{L6})_3]^{3+}$ (Fig. 3(c)). Related spectrophotometric titrations of **L7** (10^{-4} mol dm^{-3}) with $Ln(CF_3SO_3)\cdot xH_2O$ (Ln = La, Eu, Lu, Y, x = 2–4; Ln : **L7** = 0.1–2.0) shows the formation of only three absorping species assigned to **L7** and $[Ln(\mathbf{L7})n]^{3+}$ (n = 1, 2), and corresponding to equilibria (4) and (5) (Table 1). Any attempts to introduce $[Ln(\mathbf{L7})_3]^{3+}$ in the non-linear fitting process fail, which suggests that the terminal dibenzylamine groups are too bulky to allow the wrapping of three strands in the final triple-helical complexes.

A parallel ESI-MS titration performed in the same conditions for Ln = Lu confirms the exclusive formation of 1 : 1 complexes $([Lu(\mathbf{L7})]^{3+}$ at m/z = 583.6 and its adduct ions $[Lu(\mathbf{L7})(CF_3SO_3)_m]^{(3-m)+}$, m = 1, 2) and 1 : 2 complexes $([Lu(\mathbf{L7})_2(CF_3SO_3)_m]^{(3-m)+}$, m = 1, 2). Traces of $[Lu(\mathbf{L7})_3(CF_3SO_3)]^{2+}$ (m/z = 950.1) can be only detected in large excess of ligand, but its quantity in solution is expected to be negligible since the efficiency of the cationization process is maximum for the 1 : 3 saturated complexes.[27] We can thus safely ascribe the stepwise decrease of β_{13}^{Ln} when going from **L5** to **L6,** and its disappearance for **L7,** to the increased interstrand steric repulsions provided by the terminal tertiary amide groups in the final triple-helical complexes $[Ln(\mathbf{Li})_3]^{3+}$ (i = 5–7). It is also worth noting that β_{11}^{Ln} and β_{12}^{Ln} for **L7** are (i) significantly smaller than those found for **L5** and **L6** and (ii) deviate from the classical electrostatic trend (Fig. 3(a) and (b)). Both effects can be traced back to the steric bulk of the dibenzylcarboxamide side arms in **L7** which strongly limits the access of the tridentate cavity for the complexation of Ln^{III}.

In order to support our speciation in solution, we have performed ^1H NMR titrations of **L*i*** (0.15 mol dm^{-3}, i = 6, 7) with $Ln(CF_3SO_3)\cdot xH_2O$ (Ln = La, Lu, Y, x = 2–4; Ln : **L*i*** = 0.25–1.0) in CD_3CN. For **L6**, we observe the successive formation of three different complexes in agreement with the speciation calculated with the stability constants collected in Table 1 (Fig. 4).

The observation of two septuplets for the methine protons H5 and H8 combined with two doublets for the enantiotopic methyl groups H6–H7 and H9–H10 (see Fig. 1 for the numbering scheme) in $[Ln(\mathbf{L6})]^{3+}$ is reminiscent of the C_{2v}-symmetrical arrangement found in the free ligand, but the significant downfield shifts of the protons H1 and H2 (Fig. 4(a)) is diagnostic for the complexation of Ln^{III} to the tridentate binding unit in its *anti-anti* conformation.[19] The coordination sphere in $[Ln(\mathbf{L6})]^{3+}$ is completed with slow exchanging solvent molecules among which coordinated water molecules can be detected at 6.05 ppm. The 1 : 2 complexes $[Ln(\mathbf{L6})_2]^{3+}$ exhibit C_2-symmetry in agreement with the observation of (i) two non-equivalent signals for the meta protons of the pyridine ring H2 and H2′, (ii) four different heptuplets for the methine protons H5 and H8 (Fig. 4(a)) and (iii) eight diastereotopic methyl protons for H6, H7, H9, H10. A single twofold axis interconverts the two ligands in $[Ln(\mathbf{L6})_2]^{3+}$, but no other dynamically average symmetry element is observed on the NMR time scale. Finally, $[Ln(\mathbf{L6})_3]^{3+}$ is almost quantitatively formed for a ratio Ln : **L6** = 1 : 3 and the reduced number of signals is compatible with D_3-symmetrical triple helical complexes (two different heptuplets for the methine protons H5 and H8 and four diastereotopic methyl protons for H6, H7, H9, H10, Fig. 4(a)).[19] In excess of ligand (Ln : **L6** = 1 : 4), the non-coordinated **L6** provides well-defined and separated signals, thus pointing to (i) the absence of complexes with **L6** : Ln > 3, and (ii) the existence of inert $[Ln(\mathbf{L6})_3]^{3+}$ complexes on the NMR time scale at room temperature. Variable-temperature data show coalescence for the intermolecular ligand exchange process (eqn. (7)) occurring at T_c = 303 K (Ln = La), 348 K (Ln = Y) and >350 K (Ln = Lu) in CD_3CN, thus leading to $\Delta G^{\neq}$(Ln = La) = 64(2) kJ mol^{-1},

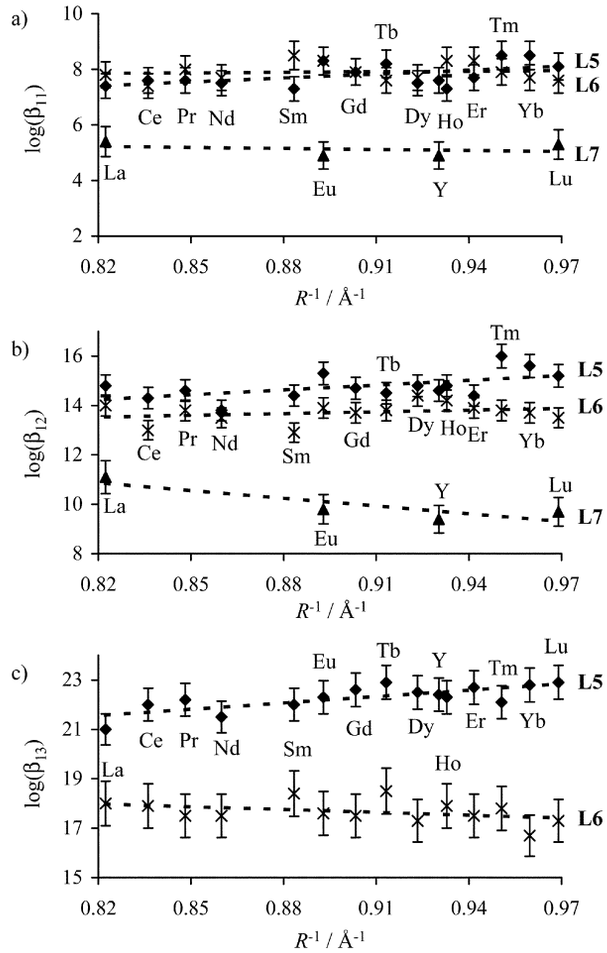

Fig. 3 Cumulatives stability constants $\log(\beta_{1n}^{Ln})$ for the formation of (a) $[Ln(\mathbf{Li})]^{3+}$ (i = 5: ◆, i = 6: X, i = 7: ▲), (b) $[Ln(\mathbf{Li})_2]^{3+}$ (i = 5: ◆, i = 6: X, i = 7: ▲) and (c) $[Ln(\mathbf{Li})_3]^{3+}$ (i = 5: ◆, i = 6: X) as a function of the inverse of nine-coordinate lanthanide radii (R^{-1})[29] (acetonitrile, 293 K). The linear trendlines are only guides for the eyes.

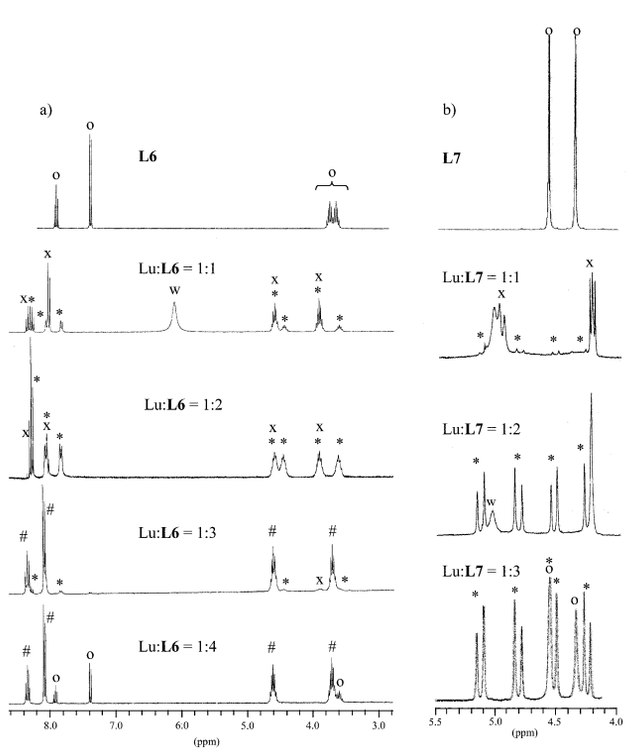

Fig. 4 Part of the ^1H NMR spectra obtained upon titration of (a) **L6** and (b) **L7** with $Lu(CF_3SO_3)_3\cdot 2H_2O$ (CD_3CN, 298 K). O = **L*i***, X = $[Lu(\mathbf{Li})]^{3+}$, * = $[Lu(\mathbf{Li})_2]^{3+}$ and # = $[Lu(\mathbf{Li})_3]^{3+}$.

$\Delta G^{\neq}$(Ln = Y) = 75(2) kJ mol^{-1} and $\Delta G^{\neq}$(Ln = Lu) > 75 kJ mol^{-1} calculated with eqns. (1)–(3) and X = 2.3 for a difference in population of Δp = 0.5 between the exchangeable sites. A similar mathematical treatment for the same intermolecular exchange process observed in [Ln(dipicolinate)$_3$]$^{3-}$ in water gives $\Delta G^{\neq}$(Ln = La) < 59 kJ mol^{-1}, $\Delta G^{\neq}$(Ln = Y) = 68(1) kJ mol^{-1} and $\Delta G^{\neq}$(Ln = Lu) = 74(2) kJ mol^{-1}.[28] This confirms that the bulky ligand **L6** is compatible with the formation of well-defined triple-helical complexes [Ln(**L6**)$_3$]$^{3+}$ in acetonitrile which are even more inert toward intermolecular ligand-exchange processes than [Ln(dipicolinate)$_3$]$^{3-}$.

$$[Ln(\mathbf{L6})_3]^{3+} + \mathbf{L6}^* \rightleftarrows [Ln(\mathbf{L6})_2(\mathbf{L6}^*)]^{3+} + \mathbf{L6} \qquad (7)$$

The parallel ^{1}H NMR titrations of **L7** with Ln(CF$_3$SO$_3$)·xH$_2$O (Ln = La, Lu, Y, x = 2–4) in CH$_3$CN show the successive formation of only two complexes corresponding to [Ln(**L7**)]$^{3+}$ (C_{2v}-symmetry) and [Ln(**L7**)$_2$]$^{3+}$ (D_2 or C_{2h} symmetry) in agreement with spectrophotometric data (Fig. 4(b)). For **L7** : Ln = 3, we do not detect significant amounts of 1 : 3 complexes (<3%, limit of detection with ^{1}H NMR), and the ^{1}H NMR spectrum corresponds to a mixture of [Ln(**L7**)$_2$]$^{3+}$ and **L7** in a 2 : 1 ratio (ligand speciation, Fig. 4(b)). Variable-temperature NMR data show no coalescence in the temperature range accessible in CD$_3$CN (233–343 K), but T_c = 413 K for Ln = Lu in CD$_3$NO$_2$ thus leading to $\Delta G^{\neq}$(Ln = Lu) = 86(2) kJ mol^{-1} for the intermolecular exchange process modeled with eqn. (8) (Δp = 0.33, X = 2.698 in eqn. (3)).

$$[Ln(\mathbf{L7})_2]^{3+} + \mathbf{L7}^* \rightleftarrows [Ln(\mathbf{L7})(\mathbf{L7}^*)]^{3+} + \mathbf{L7} \qquad (8)$$

In conclusion, the ^{1}H NMR titration confirm the speciation evidenced by spectrophotometry with the formation of 1 : 1 and 1 : 2 complexes with both ligands **L6** and **L7**, while 1 : 3 complexes is restricted to the less bulky receptor **L6**. Interestingly, [Ln(**L6**)$_3$]$^{3+}$ and [Ln(**L7**)$_2$]$^{3+}$ display comparable activation energies for intermolecular ligand-exchange processes despite their different stoichiometries. A strict comparison between the lanthanide complexes of **L6** and **L7** is thus limited to the 1 : 2 complexes, and it is unexpected that [Ln(**L6**)$_2$]$^{3+}$ possesses an average C_2-symmetry on the NMR time scale, while [Ln(**L7**)$_2$]$^{3+}$ is characterized by average D_2 or C_{2h} symmetries. Reliable structural models in solution will be proposed after the description of the molecular solid-state structures found for 1 : 2 complexes (*vide infra*, Fig. S3, ESI†), but we tentatively assign the average lower symmetry observed for [Ln(**L6**)$_2$]$^{3+}$ on the NMR time scale to the more rigid coordination of the ligand (compared with [Ln(**L7**)$_2$]$^{3+}$) which limits the access (and decreases kinetic exchange rates) of ancillary solvent molecules and/or counter-anions. In this context, it is worth noting that the analogous rigid 1 : 1 complexes [Ln(**L4**)(NO$_3$)$_3$] display anomanously slow anion-exchange processes in solution, thus leading to the observation of separate spectra for [Ln(**L4**)(NO$_3$)$_3$] and [Ln(**L4**)(NO$_3$)$_2$]$^+$ on the NMR time scale.[17a,c]

Isolation and characterization of 1 : 2 complexes [Ln(L*i*)$_2$](CF$_3$SO$_3$)$_3$·xH$_2$O·yTHF (*i* = 6, 7; Ln = Eu, Gd, Tb, Lu)

Diffusion of diethyl ether into concentrated THF solutions containing stoichiometric mixtures of **L6** or **L7** (2 equiv.) and Ln(CF$_3$SO$_3$)·xH$_2$O (Ln = Eu, Gd, Tb, Lu, x = 2–4, 1 equiv.) provides microcrystalline powders of [Ln(**L6**)$_2$](CF$_3$SO$_3$)$_3$·xH$_2$O·yTHF (Ln = Eu, x = 2, y = 0: **1**; Ln = Gd, x = y = 0: **2;** Ln = Tb, x = y = 0: **3;** Ln = Lu, x = 0, y = 1.5: **4**) and [Ln(**L7**)$_2$](CF$_3$SO$_3$)$_3$·xH$_2$O·yTHF (Ln = Eu, x = 1, y = 0: **5**; Ln = Gd, x = 0, y = 2: **6;** Ln = Tb, x = 3, y = 0: **7;** Ln = Lu, x = 1, y = 0: **8**) in 74–84% yields. Elemental analyses support the proposed formulations (Table S2, ESI†), and dissolution in acetonitrile gives ESI-MS and ^{1}H NMR data identical to those obtained upon direct titrations with Ln : L*i* = 1 : 2. Fragile solvated monocrystals suitable for X-ray diffraction studies have been obtained for [Eu(**L6**)$_2$(H$_2$O)$_2$(CF$_3$SO$_3$)](CF$_3$SO$_3$)$_2$(THF)$_{1.5}$ (**9**) and [Gd(**L7**)$_2$(H$_2$O)$_2$(CF$_3$SO$_3$)](CF$_3$SO$_3$)$_2$(^{t}BuOMe)$_2$ (**10**) upon ultra slow diffusion of various dialkylether into concentrated solutions of **1** in THF, respectively of **6** in propionitrile.

Crystal and molecular structure of [Eu(L6)$_2$(H$_2$O)$_2$(CF$_3$SO$_3$)](CF$_3$SO$_3$)$_2$(THF)$_{1.5}$ (9) and [Gd(L7)$_2$(H$_2$O)$_2$(CF$_3$SO$_3$)](CF$_3$SO$_3$)$_2$(^{t}BuOMe)$_2$ (10)

The crystal structures of **9** and **10** confirm the formation of 1 : 2 complexes in which Ln^{III} is coordinated to two tridentate ligands, two water molecules and one monodentate triflate anion to give the nine-coordinate cations [Eu(**L6**)$_2$(H$_2$O)$_2$(CF$_3$SO$_3$)]$^{2+}$ and [Gd(**L7**)$_2$(H$_2$O)$_2$(CF$_3$SO$_3$)]$^{2+}$. The non-complexed solvent molecules and ionic triflates display some weak hydrogen bonds with the coordinated water molecules but show no other feature of interest. Fig. 5 shows the numbering schemes for the two cations, and selected bond-distances and angles are given in Table 2.

Except for the slight contraction expected when going from Ln = Eu in **9** to Ln = Gd in **10** (relative contraction = 1.2% for nine-coordinate metals),[29] the molecular structures of the two cations are almost superimposable (Fig. 6). The coordination sphere of Ln^{III} can be best described as a distorted monocapped square antiprism (MSA) in which O2a, N1a, O2b, N1b and O1a, O1c, O1b, O2w define, respectively, the lower and upper tetragonal faces of the approximate antiprism, the latter being capped by O1w (Scheme 2 and Fig. S4, ESI†). The two tetragonal faces are almost paralell (interplane angles: 2° in **9** and 3° in **10**) and separated by 2.31 Å (**9**) and 2.29 Å (**10**), Ln^{III} being located closer to the capped face (0.67 Å for **9** and 0.64 Å for **10**). A geometrical analysis based on the angles ϕ, θ_i and ω_{ij} defined in Scheme 2 is given in Table 3. It shows that the coordination spheres indeed fit the main criteria required for an approximate MSA arrangement, except for the different flatenning of the two tetrapodes (θ = 74(5)° for the upper O1a, O1c, O1b, O2w tetrapode and θ= 50(8)° for the lower O2a, N1a, O2b, N1b tetrapode, Table 3) which results from the shift of Ln^{III} toward the capping oxygen atom O1w.

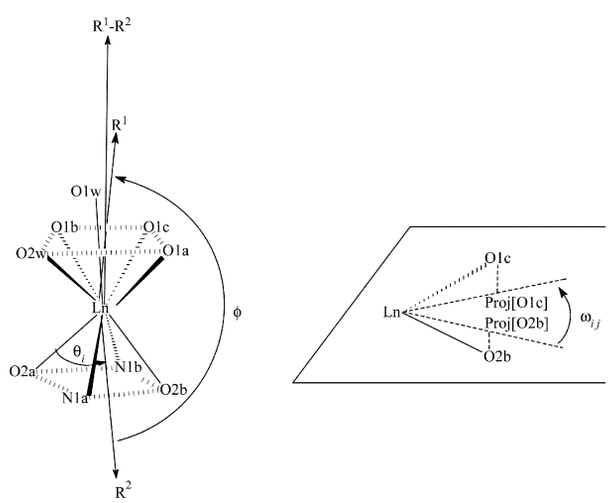

Scheme 2

The Ln–N(pyridine), Ln–O(amide) and Ln–O(water) bond distances are standard[30] and they closely match those reported for [Eu(**L5**)$_3$](CF$_3$SO$_3$)$_3$.[19] The ionic radii calculated according to Shannon's definition[29] with r(N) = 1.46 Å[29], r(O) = 1.35 Å for water and r(O) = 1.31 Å for coordinated amide and triflate oxygen atoms,[31] amount to $R_{Eu(III)}$ = 1.111 Å in **9** and $R_{Gd(III)}$ = 1.098 Å in **10**, which satisfyingly fit the expected ionic radii for nine-coordinate Eu^{III} (1.120 Å) and Gd^{III} (1.107 Å).[29] This

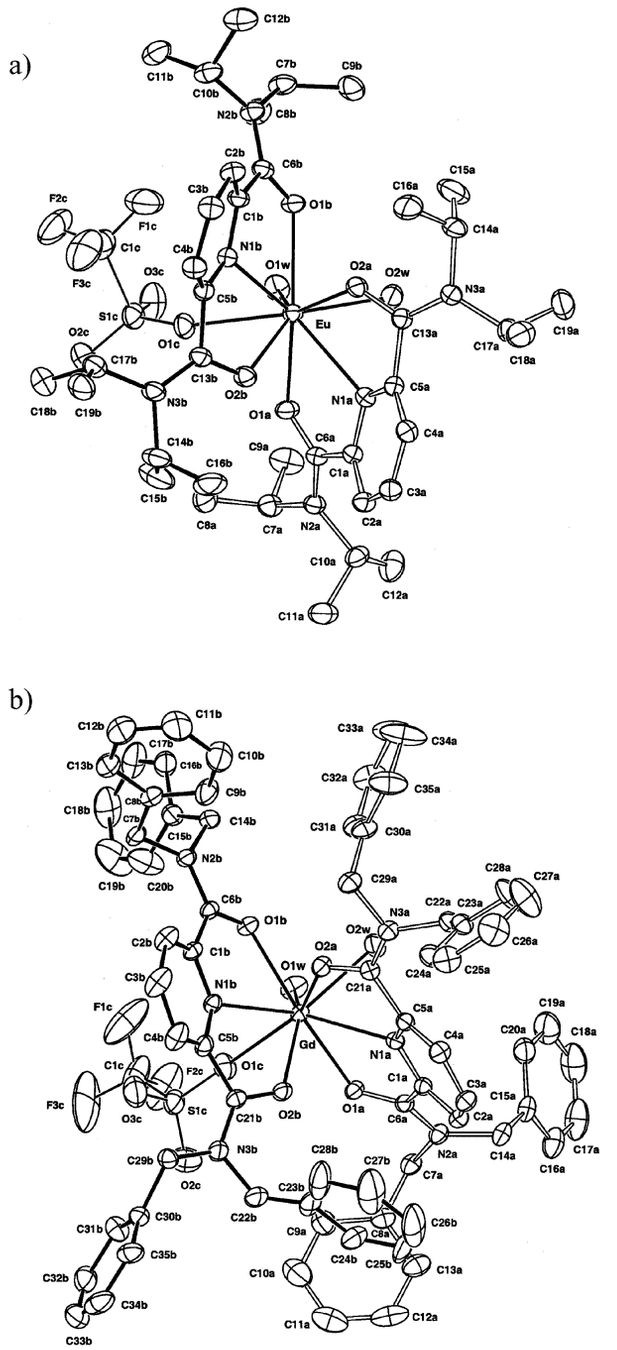

Fig. 5 ORTEP views of the molecular structures of the cations (a) $[Eu(\mathbf{L6})_2(H_2O)_2(CF_3SO_3)]^{2+}$ (**9**) and (b) $[Gd(\mathbf{L7})_2(H_2O)_2(CF_3SO_3)]^{2+}$ (**10**) along the Ln–O1w bond with atomic numbering scheme. Ellipsoids are represented at 40% probability level for **9** and 30% probability level for **10**.

points to minor steric constraints affecting the structure of the 1 : 2 complexes whatever the size of the terminal groups connected to the carboxamide side arms (isopropyl in **9** and benzyl in **10**). Finally, the careful consideration of the molecular structures of $[Eu(\mathbf{L6})_2(H_2O)_2(CF_3SO_3)]^{2+}$ and $[Gd(\mathbf{L7})_2(H_2O)_2(CF_3SO_3)]^{2+}$ suggests the existence of a pseudo-two-fold axis passing throug Ln-O1w according that the coordinated triflate anions are replaced with water molecules (Fig. 5). Since this exchange process is likely to occur in solution with the average fixation of three solvent molecules, we expect an average C_2-symmetry on the NMR time scale under slow exchange regime as observed for $[Ln(\mathbf{L6})_2]^{3+}$in CD_3CN (Fig. S3(a), ESI †). The higher symmetry evidenced for $[Ln(\mathbf{L7})_2]^{3+}$ in solution implies (i) a partial re-orientation of the two tridentate ligands providing a two-fold axis passing through the pyridine rings of each

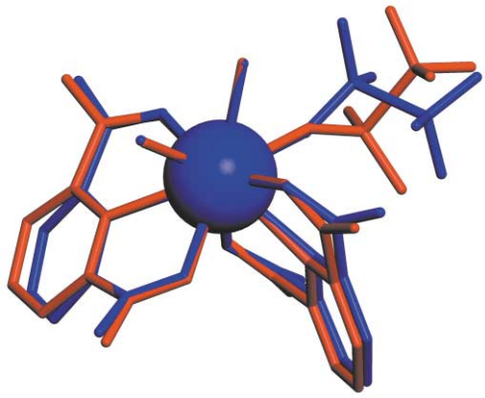

Fig. 6 Perspective view of the optimized superposition of the two coordination spheres of (a) $[Eu(\mathbf{L6})_2(H_2O)_2(CF_3SO_3)]^{2+}$ (in blue) and (b) $[Gd(\mathbf{L7})_2(H_2O)_2(CF_3SO_3)]^{2+}$ (in red). The terminal isopropyl and benzyl groups have been omitted for clarity.

ligand and (ii) a faster dynamic exchange of the solvent molecules which eventually occupy average interconverting positions within the meridional plane (Fig. S3(b) and (c), ESI †). Depending on the relative orientation of the pyridine rings, the average solution structures correspond to either C_{2h}-symmetry (≡ meridional coordination) or D_2-symmetry (≡ double-stranded helix, Fig. 3(b) and (c), ESI †).

Photophysical properties of the 1 : 2 complexes $[Ln(L6)_2](CF_3SO_3)_3$ (Ln = Eu, 1; Ln = Gd, 2; Ln = Tb, 3; Ln = Lu, 4) and $[Ln(L7)_2](CF_3SO_3)_3$ (Ln = Eu, 5; Ln = Gd, 6; Ln = Tb, 7; Ln = Lu, 8) in solution. Sensitization processes, antenna effect and quantum yields

According to the stability constants determined for $[Eu(\mathbf{L}i)_n]^{3+}$ in acetonitrile (i = 6, 7; n = 1, 2, Table 1), we calculate that the formation of more than 80% of $[Eu(\mathbf{L}i)_2]^{3+}$ (ligand speciation) for a stoichiometric ratio Eu : **L***i* = 1 : 2, requires a total ligand concentration larger than 2×10^{-3} mol dm^{-3} (Fig. S5, ESI †). We have therefore performed photophysical studies by using 10^{-3} mol dm^{-3} solutions of complexes **1**–**8** as a compromise for which decomplexation is minimized, but self-quenching is not too dramatic. The absorption spectra of the free ligands **L5**,[19] **L6** and **L7** in the 41000–25000 cm^{-1} range are very similar and show a broad maximum centered around 37000 cm^{-1}, and assigned to n ⟶ π* and π ⟶ π* transitions centered onto the pyridine-dicarboxamide units (Table 4).[19] Since toluene exhibits only weak structured n ⟶ π* transitions in this domain ($\varepsilon \approx 120$–260 M^{-1} cm^{-1}),[32] the benzyl groups in **L7** and **L8** are not expected to strongly contribute to the low-energy part of the absorption spectrum, and our results suggest that their connections to the N-atom of the carboxamide units do not affect their electronic properties.

Upon complexation to Ln^{III} in the 1 : 2 complexes $[Ln(\mathbf{L}i)_2](CF_3SO_3)_3$ (**1**–**8**), the intensity of the molar absorbance per ligand significantly increases with the concomitant appearance of two broad maxima around 40700 and 34500 cm^{-1} (Fig. S2, ESI, † Table 4).[19] Excitation *via* the ligand-centered n,π ⟶ π* transitions for $[Eu(\mathbf{L}i)_2]^{3+}$ (i = 6, **1** and i = 7, **5**) and $[Tb(\mathbf{L}i)_2]^{3+}$ (i = 6, **3** and i = 7, **7**) produce sizeable metal-centered luminescence characterized by sharp bands associated with $^5D_0 \longrightarrow {}^7F_J$ (J = 0–6) transitions for Ln = Eu and $^5D_4 \longrightarrow {}^7F_J$ (J = 6–0) transitions for Ln = Tb. No residual emission of the ligand-centered singlet ($^1\pi\pi^*$) and triplet ($^3\pi\pi^*$) can be detected in solution (Fig. 7(a) and (b)), but the observed quantum yields remain modest for these complexes ($3 \times 10^{-5} \leq \Phi_{tot}^{Ln} \leq 10^{-2}$, Table 5), and comparable to those found for the saturated triple-helical nine-coordinate $[Ln(\mathbf{L5})_3]^{3+}$ in the same conditions.[19] The long lifetimes ($1.8 \leq \tau_{obs} \leq 2.8$ ms, Table 5) measured for the Eu($^5D_0$) excited level in $[Eu(\mathbf{L}i)_2]^{3+}$ (i = 6, 7) and Tb($^5D_4$) in $[Tb(\mathbf{L}i)_2]^{3+}$ (i = 6, 7) again match those reported for the

Table 2 Selected bond lengths (Å) and bond angles (°) in $[Eu(\mathbf{L6})_2(H_2O)_2(CF_3SO_3)](CF_3SO_3)_2(THF)_{1.5}$ (**9**) and $[Gd(\mathbf{L7})_2(H_2O)_2(CF_3SO_3)](CF_3SO_3)_2(^tBuOMe)_2$ (**10**)

$[Eu(\mathbf{L6})_2(H_2O)_2(CF_3SO_3)](CF_3SO_3)_2$			$[Gd(\mathbf{L7})_2(H_2O)_2(CF_3SO_3)](CF_3SO_3)_2$		
	Ligand a	Ligand b		Ligand a	Ligand b
Eu–O1	2.386(3)	2.419(2)	Gd–O2	2.485(3)	2.389(3)
Eu–N1	2.594(3)	2.600(3)	Gd–N1	2.586(3)	2.592(3)
Eu–O2	2.403(3)	2.463(3)	Gd–O1	2.411(2)	2.377(3)
O1–Eu–N1	63.41(9)	63.78(9)	O1–Gd–N1	63.48(9)	62.3(1)
N1–Eu–O2	62.25(9)	62.3(1)	N1–Gd–O2	62.40(9)	63.67(9)
O1–Eu–O2	125.23(9)	126.02(9)	O1–Gd–O2	125.45(9)	125.89(9)
Eu–O1c	2.459(3)		Gd–O1c	2.410(3)	
Eu–O1w	2.438(3)		Gd–O1w	2.430(3)	
Eu–O2w	2.444(3)		Gd–O2w	2.409(3)	
O1c–Eu–O1w	71.2(1)		O1c–Gd–O1w	69.6(1)	
O1w–Eu–O2w	70.8(1)		O1w–Gd–O2w	70.3(3)	
O1c–Eu–O2w	141.4(1)		O1c–Gd–O2w	139.8(1)	

Table 3 Selected structural data for the lanthanide coordination spheres in $[Eu(\mathbf{L6})_2(H_2O)_2(CF_3SO_3)](CF_3SO_3)_2(THF)_{1.5}$ (**9**) and $[Gd(\mathbf{L7})_2(H_2O)_2(CF_3SO_3)](CF_3SO_3)_2(^tBuOMe)_2$ (**10**)

	9	**10**	Perfect MSA [b]
Angles ϕ [a]/°			
R^1–Ln–R^2	174.7	176.9	180
Angles θ_i [a]/° (distal tetrapodes)			
R^1–Ln–O1b	71.4	78.2	*a*
R^1–Ln–O1a	81.6	76.6	*a*
R^1–Ln–O1c	71.8	71.3	*a*
R^1–Ln–O2w	69.8	68.6	*a*
R^2–Ln–N1b	58.1	56.3	*a*
R^2–Ln–O2b	41.8	42.2	*a*
R^2–Ln–N1a	59.2	58.1	*a*
R^2–Ln–O2a	39.0	38.4	*a*
Angles ω_{ij} [a]/°			
Proj[O1a]–Ln–Proj[O2b] [c]	51.5	49.8	45
Proj[O1a]–Ln–Proj[N1a]	46.5	46.7	45
Proj[O1b]–Ln–Proj[N1b]	43.5	44.5	45
Proj[O2w]–Ln–Proj[N1a]	48.7	49.8	45
Proj[O1c]–Ln–Proj[O2b]	27.8	33.8	45
Proj[O1c]–Ln–Proj[N1b]	57.3	54.1	45
Proj[O2w]–Ln–Proj[O2a]	33.3	33.8	45
Proj[O1b]–Ln–Proj[O2a]	48.6	47.9	45

[a] For the definition of ϕ, θ_i and ω_{ij}, see Scheme 2. The error in the angles is typically 0.5°. [b] Perfect MSA = monocapped square antiprism. [c] Proj[O(*i*)] and Proj[N(*i*)] are the projections of O(*i*) and respectively N(*i*) along the R^1–R^2 direction onto a perpendicular plane passing through the lanthanide atom. R^1 = Ln–O1a + Ln–O1b + Ln–O1c + Ln–O2w and R^2 = Ln–O2a + Ln–O2b + Ln–N1a + Ln–N1b.

related saturated complexes $[Ln(\mathbf{L5})_3]^{3+}$ and point to the absence of water molecule in the first coordination spheres. Since two water molecules are bound to Ln^{III} in the crystal structures of $[Eu(\mathbf{L6})_2(H_2O)_2(CF_3SO_3)]^{2+}$ and $[Gd(\mathbf{L7})_2(H_2O)_2(CF_3SO_3)]^{2+}$, we conclude that solvent exchange occur in solution and that the water molecules coordinated in the solid-state are replaced with CH_3CN and/or triflate counter-anions in acetonitrile.

A thorough comparison beween $[Ln(\mathbf{L6})_2]^{3+}$ and $[Ln(\mathbf{L7})_2]^{3+}$ (Ln = Eu and Tb respectively) reveals that $[Ln(\mathbf{L7})_2]^{3+}$ exhibit quantum yields improved by factors of 4 (Ln = Tb) and 8 (Ln = Eu, Table 5). The origin of this beneficial effect is difficult to assign because the overall antenna effect involves a multistep mechanism in which (i) UV light is first collected by the singlet

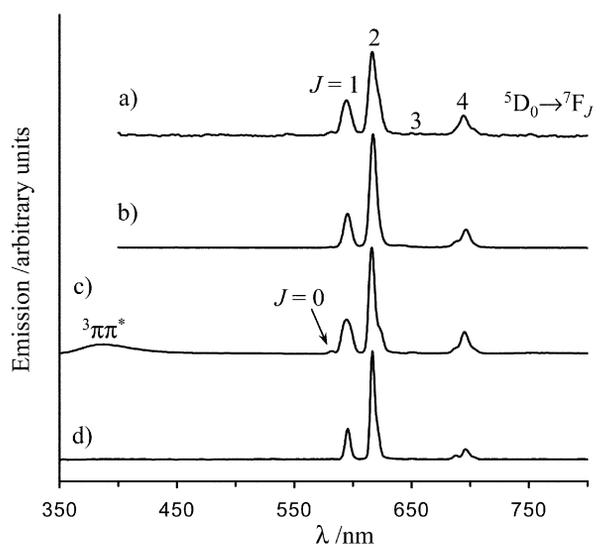

Fig. 7 Time-resolved phosphorescence spectra (delay 0.1 ms) of (a) $[Eu(\mathbf{L6})_2]^{3+}$ (10^{-3} mol dm^{-3} in acetonitrile, λ_{exc} = 32780 cm^{-1}, 293 K), (b) $[Eu(\mathbf{L7})_2]^{3+}$ (10^{-3} mol dm^{-3} in acetonitrile, λ_{exc} = 31250 cm^{-1}, 293 K), (c) $[Eu(\mathbf{L6})_2](CF_3SO_3)_3\cdot 2H_2O$ (**1**, λ_{exc} = 42194 cm^{-1}, 77 K) and (d) $[Eu(\mathbf{L7})_2](CF_3SO_3)_3\cdot H_2O$ (**5**, λ_{exc} = 39215 cm^{-1}, 77 K).

ligand-centered states, then (ii) $^1\pi\pi^* \longrightarrow {}^3\pi\pi^*$ conversion occurs (η_{ISC}) followed by (iii) energy transfer from the ligand-centered to the metal-centered excited states ($^3\pi\pi^* \longrightarrow$ Ln, η_{ET}), and (iv) metal-centered visible light emission (Ln = Eu, Tb, Φ^{Ln}). The total quantum yield Φ_{tot}^{Ln} is thus given by eqn. (9)[33] and the replacement of the terminal isopropyl groups in $[Ln(\mathbf{L6})_2]^{3+}$ with benzyl groups in $[Ln(\mathbf{L7})_2]^{3+}$ may affect any step.

$$\Phi_{tot}^{Ln} = \eta_{ISC}\eta_{ET}\Phi^{Ln} = \eta_{sens}\Phi^{Ln} \quad (9)$$

Since the lanthanide luminescence step is given by $\Phi^{Ln} = \tau_{obs}/\tau_R$, and the radiative lifetimes τ_R are not expected to dramatically vary between the closely related complexes $[Ln(\mathbf{L6})_2]^{3+}$ and $[Ln(\mathbf{L7})_2]^{3+}$,[20b,33] we deduce that (i) the minor variation of the observed lifetimes (τ_{obs}, Table 5) cannot account for the observed change in the total quantum yield Φ_{tot}^{Ln}, and (ii) the sensitization process (η_{sens}) is thus slightly more efficient for $[Ln(\mathbf{L7})_2]^{3+}$. Although ligand-centered emission is too weak to be detected in solution at 293 K for $[Ln(\mathbf{Li})_2]^{3+}$ (Ln = Gd, Lu, *i* = 6, 7), we have resorted to solid-state samples of $[Ln(\mathbf{L6})_2](CF_3SO_3)_3$ (Ln = Gd, **2**; Ln = Lu, **4**) and $[Ln(\mathbf{L7})_2](CF_3SO_3)_3$ (Ln = Gd, **6**; Ln = Lu, **8**) for investigating the energies of the ligand-centered $^1\pi\pi^*$ and $^3\pi\pi^*$ excited states. At 77 K, these complexes exhibit similar broad emission bands

Table 4 Ligand-centered absorption at 293 K (10^{-3} mol dm^{-3} in acetonitrile) and emission properties at 77 K (solid state) for the ligands **L6**, **L7** and selected complexes [Ln(**L*i***)$_2$](CF$_3$SO$_3$)$_3$·xH$_2$O·yTHF (Ln = Eu, Gd, Tb, Lu; **1**–**8**)

Compound	E(n,π ⟶ π*)/cm^{-1} [a]	E(^{1}ππ*)/cm^{-1} [b]	E(^{3}ππ*)/cm^{-1} [b]	τ(^{3}ππ*)/ms
L5 [c]	37040 (7160)	[d]	[d]	[d]
L6	37040 (8500)	34540	25680	[d]
L7	37300 (6500)	34600	25910	[d]
[Lu(**L6**)$_2$](CF$_3$SO$_3$)$_3$ (**4**)	40980 (18400) 35340 (21000) 34600 (19300 sh)	34600	26040	0.11(2)
[Lu(**L7**)$_2$](CF$_3$SO$_3$)$_3$ (**8**)	40650 (23680) 34840 (20460 br)	34540	25940	0.12(2)
[Gd(**L6**)$_2$](CF$_3$SO$_3$)$_3$ (**2**)	40650 (19400) 35460 (21500) 34600 (19100 sh)	34540	25940	0.12(3)
[Gd(**L7**)$_2$](CF$_3$SO$_3$)$_3$ (**6**)	40980 (24900) 34840 (21450 br)	34600	25940	0.12(2)
[Eu(**L6**)$_2$](CF$_3$SO$_3$)$_3$ (**1**)	40650 (21600) 35460 (23400) 34600 (20700 sh)	34480	25810	[d]
[Eu(**L7**)$_2$](CF$_3$SO$_3$)$_3$ (**5**)	41150 (24800) 34840 (20460 br)	[e]	[f]	[d]
[Tb(**L6**)$_2$](CF$_3$SO$_3$)$_3$ (**3**)	40650 (20260) 35460 (22840) 34700 (20630 sh)	34600	26100	[d]
[Tb(**L7**)$_2$](CF$_3$SO$_3$)$_3$ (**7**)	41150 (24800) 34840 (20460 br)	34600	25940	[d]

[a] 10^{-3} mol dm^{-3} in acetonitrile; sh = soulder. br = broad. Energies are given for the maximum of the band envelope and the molar absorption coefficient (ε) is given in parentheses in M^{-1} cm^{-1}. [b] Data obtained from the emission spectra at 77 K recorded on solid-state samples. [c] Taken from ref. 19. [d] Not determined. [e] Quenched by efficient **L7** (^{1}ππ*) ⟶ Eu(III) transfer and/or by intersystem crossing **L7** (^{1}ππ*) ⟶ **L7** (^{3}ππ*). [f] Quenched by efficient **L7** (^{3}ππ*) ⟶ Eu(III) transfer.

Table 5 Absolute quantum yields (Φ) and lifetimes (τ) of the Eu(^{5}D$_0$) excited level in [Eu(**L*i***)$_2$](CF$_3$SO$_3$)$_3$ (i = 6, **1**; i = 7 : **5**) and Tb(^{5}D$_4$) in [Tb(**L*i***)$_2$](CF$_3$SO$_3$)$_3$ (i = 6, **3**; i = 7 : **7**), and in related complexes (10^{-3} mol dm^3 in acetonitrile, 293 K)

Compound	$\tilde{\nu}_{ex}$/cm^{-1}	Φ	τ/ms
[Eu(**L6**)$_2$](CF$_3$SO$_3$)$_3$ (**1**)	32785	3.3×10^{-5}	2.03(1)
[Eu(**L7**)$_2$](CF$_3$SO$_3$)$_3$ (**5**)	31250	2.2×10^{-4}	2.78(1)
[Tb(**L6**)$_2$](CF$_3$SO$_3$)$_3$ (**3**)	31750	2.8×10^{-3}	2.26(2)
[Tb(**L7**)$_2$](CF$_3$SO$_3$)$_3$ (**7**)	31250	9.9×10^{-3}	1.82(2)
[Eu(**L5**)$_3$](CF$_3$SO$_3$)$_3$ [a]	32051	8.6×10^{-5}	2.42(4)
[Tb(**L5**)$_3$](CF$_3$SO$_3$)$_3$ [a]	31055	3.5×10^{-2}	1.85(3)
[Eu(**L1**)$_3$](ClO$_4$)$_3$ [b]	26955	1.3×10^{-2}	2.71(3)
[Tb(**L1**)$_3$](ClO$_4$)$_3$ [b]	27470	4.7×10^{-2}	1.21(3)

[a] Taken from ref. 19. [b] Taken from ref. 40.

originating from ^{1}ππ* at 34600 cm^{-1} and ^{3}ππ* at 25900 cm^{-1} (Table 4, Fig. S6, ESI †). The large energy gap $\Delta E = E(^1\pi\pi^*) - E(^3\pi\pi^*) = 8700$ cm^{-1} ensures an efficient driving force for the intersystem crossing process (5000 cm^{-1} is considered as a minimal gap to generate sizeable η_{ISC}).[34] However, the rather short lifetimes of the triplet states in [Ln(**L*i***)$_2$](CF$_3$SO$_3$)$_3$ (i = 6, 7) ($\tau(^3\pi\pi^*) = 110$–120 μs, Table 4) contrast with those reported for similar coordinated *ONO* tridentate binding units in nonadentate Lu–podate ($\tau(^3\pi\pi^*) = 27$ ms) and Gd–podate ($\tau(^3\pi\pi^*) = 3$ ms).[35] This points to efficient de-excitation pathways of the ^{3}ππ* states in [Ln(**L*i***)$_2$](CF$_3$SO$_3$)$_3$ (i = 6, 7, spin–orbit mixing, paramagnetic effect, vibrational quenching)[36] which strongly limit the sensitization process.[37] Moreover, the systematic observation of residual ^{1}ππ* and ^{3}ππ* emissions for [Ln(**L6**)$_2$](CF$_3$SO$_3$)$_3$ (Ln = Eu, Tb, Fig. 7(c)) and [Tb(**L7**)$_2$](CF$_3$SO$_3$)$_3$ (Table 4) indicates poorly efficient ligand ⟶ Ln^{III} energy transfers which can be tentatively assigned to a poor match between the energies of the ligand-centered donor and metal-centered acceptor levels. Interestingly, residual ^{1}ππ* and ^{3}ππ* emissions are not detected for [Eu(**L7**)$_2$](CF$_3$SO$_3$)$_3$ (Fig. 7(d)) in agreement with slightly better energy transfer processes (η_{ET}) with **L7**, leading to larger overall quantum yields. We cannot propose any obvious origin for this effect, but a better match of the donor and acceptor energy levels in phonon-assisted energy transfers could benefit from the replacement of isopropyl groups in **L6** (aliphatic CC and CH vibrations) with benzyl groups in **L7** (aromatic CC and CH vibrations).

The case of the tridentate ligand L8 fitted with secondary amide side arms: crystal and molecular structure of [Tb(**L8**)$_3$]$_2$-(CF$_3$SO$_3$)$_6$(CH$_3$CH$_2$CN)$_3$(H$_2$O) (**11**)

Because of the considerable kinetic interness provided by the intramolecular hydrogen bonds which stabilize **L8** in its *syn-syn-ZZ* conformation (Fig. 1), the complexation processes with Ln(CF$_3$SO$_3$)·xH$_2$O are extremely slow and we were unable to collect satisfying spectrophotometric data under thermodynamic equilibrium. Mixtures containing Ln : **L8** ratios of 1 : 1, 1 : 2 and 1 : 3 in CD$_3$CN and equilibrated for one week (Ln = La, Y, Lu, total ligand concentration: 10^{-2} mol dm^{-3}) provide intractable ^{1}H NMR spectra suggesting the formation of complexes [Ln(**L8**)$_n$]$^{3+}$ (n = 1, 2, 3, respectively) in which **L8** adopts the *anti-anti* conformation combined with three different arrangements of the terminal secondary amides (*EE*, *EZ* and *ZZ*). For the triple-helical complexes [Ln(**L8**)$_3$]$^{3+}$, we calculate that a statistical 1 : 2 : 1 distribution of the *EE* : *EZ* : *ZZ* conformers within each ligand strand produces 13 different inert isomeric complexes in variable proportions (1.5–19%, Table S3, ESI †). It is thus not surprising that the ^{1}H NMR data escape a straightforward interpretation, and the speciation in solution was not pursued. Interestingly, slow diffusion of light petroleum into a stoichiometric mixture of **L8** (3 equiv.) and Tb(CF$_3$SO$_3$)·3H$_2$O (1 equiv.) in propionitrile produces X-ray quality prisms of [Tb(**L8**)$_3$]$_2$(CF$_3$SO$_3$)$_6$(CH$_3$CH$_2$CN)$_3$-(H$_2$O) (**11**) existing as inversion twins in various ratio for each crystals. The solvent molecules and triflate anions are not coordinated and display some disorders (see Experimental section), but show no other feature of interest. The unit cell contains two asymmetric nine-coordinate triple-helical cations [Tb(**L8**)$_3$]$^{3+}$ displaying opposite helicities and slightly different arrangements of the tridentate ligand strands (Fig. 8: Δ-[Tb(**L8**)$_3$]$^{3+}$ (**11a**: strands a, b, c) and Λ-[Tb(**L8**)$_3$]$^{3+}$ (**11b**: strands d, e, f)). Fig. 8 shows the atomic numbering scheme, Fig. 9 displays a stereoview of the two cations of the

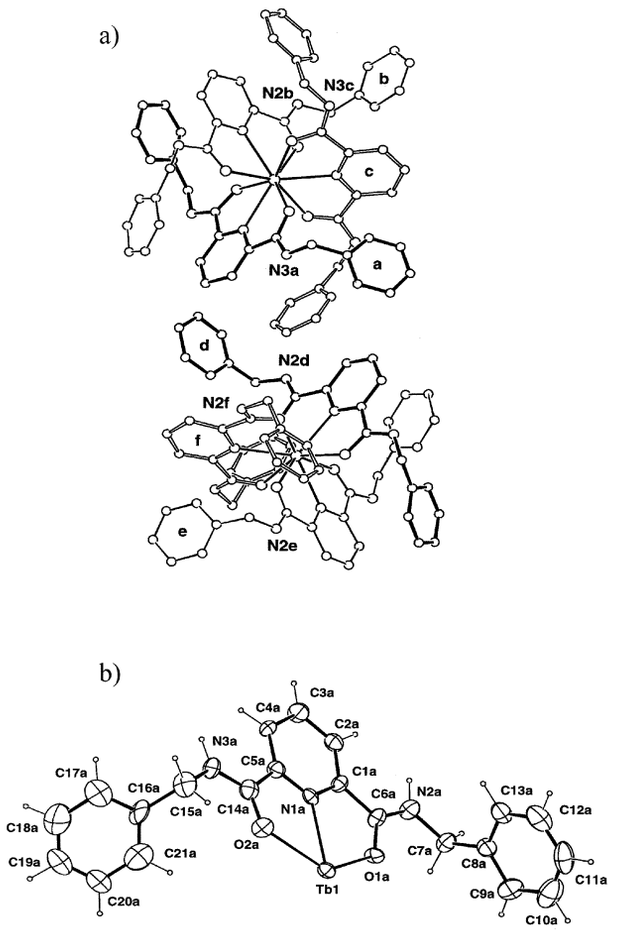

Fig. 8 (a) Perspective views of the molecular structure of the two cations of the asymmetric unit approximately along their pseudo-three-fold axis with atomic numbering scheme (Δ-[Tb(**L8**)$_3$]$^{3+}$ (**11a**: strands a–c) and Λ-[Tb(**L8**)$_3$]$^{3+}$ (**11b**: strands d–f). (b) ORTEP view of the coordinated strand *a* showing the atomic numbering scheme. Ellipsoids are represented at 40% probability level.

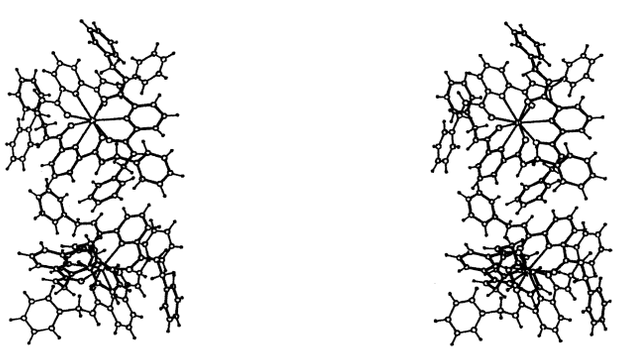

Fig. 9 Stereoview of the molecular structure of the two cations approximately along their pseudo-three-fold axis (top: **11a**, bottom: **11b**).

asymmetric unit. Selected bond angles and bond distances are collected in Table 6.

All the secondary amide groups of the six ligands exhibit *ZZ* conformations, while the benzyl groups are further oriented to produce overall *S*-shape conformations for the strands. For **11a**, the cation forms a right-handed (Δ ≡ *P*) triple-helix displaying pseudo-D_3 symmetry with the approximate three-fold axis perpendicular to the {N1a, N1b, N1c} plane, and the two-fold axes passing through C3*m*–N1*m*–Tb1 (*m* = a, b, c; Fig. 9). An opposite left-handed helicity (Λ ≡ *M*) characterizes the cation **11b** when we consider an imaginary three-fold axis perpendicular to the {N1d, N1e, N1f} plane, but the benzyl groups of strands d and f point outward this imaginary axis, while those of strand f point inward (Figs. 8 and 9). Consequently, the pseudo-C_3 is removed in **11b** and a single pseudo-two-fold axis passing through C3f–N1f–Tb2 remains. The Tb–N and Tb–O bond distances are standard,[30] and the calculation of the ionic radii (r(N) = 1.46 Å, r(O) = 1.31 Å for coordinated amide oxygen atoms)[29,31] gives R_{Tb1} = 1.067 Å and R_{Tb2} = 1.075 Å which roughly match the expected ionic radius for nine-coordinate Tb^{III} (1.095 Å).[29] The coordination spheres can be described as distorted tricapped trigonal prismatic sites (TTP) in which the oxygen atoms occupy the vertex of the prism and the three nitrogen atoms cap the rectangular faces. A classical geometrical analysis based on the angles ϕ, θ_i and ω_{ij} defined in Table S4 (ESI†)[15b,19] show very similar coordination sites for **11a** and **11b** displaying minor twists of the trigonal faces (ω_{ij} = 9–16°, perfect TTP: 0°) as found in [Eu(**L5**)$_3$]$^{3+}$ (ω_{ij} = 18–19°).[19] It is worth noting that the average flattening of the trigonal prism along the three-fold axis in **11a** (θ = 49(2)°), **11b** (θ = 47(2)°) and [Eu(**L5**)$_3$]$^{3+}$ (θ = 46(2)°) are comparable despite the extended intermolecular π-stacking interactions involving the benzyl groups in [Tb(**L8**)$_3$]$_2$(CF$_3$SO$_3$)$_6$(CH$_3$-CH$_2$CN)$_3$(H$_2$O) (**11**) (Table S5, ESI†). In the crystal of **11**, the cations [Tb(**L8**)$_3$]$^{3+}$ arrange in layers parallel to the *ac* plane. Within each layer, a compact pseudo-tetragonal network results from numerous intermolecular offset π-stacking and edge-to-face interactions involving the aromatic benzyl and pyridine rings (Table S5, Fig. S7, ESI†). However, we do not detect strong hydrogen bonds involving the amide N–H groups in contrast to those found in the free ligand **L8**. We thus conclude that the removal of two benzyl groups when going from **L7** to **L8** restores the formation of stable triple-helical complexes, but the existence of conformational isomers strongly limit characterization in solution. The crystal structure of **11** is a lucky example in which the (*ZZZ*)^3 isomer selectively crystallizes.

Conclusion

Following our pioneer work with **L5**,[19] we demonstrate here that the connection of symmetrical tertiary amide side arms at the 2- and 6-positions of the central pyridine rings provide a library of versatile tridentate binding units for the complexation of Ln^{III}. The increased steric congestion brought by the replacement of diethylamide (**L5**) with diisopropylamide (**L6**) and dibenzylamide (**L7**) decreases the affinity of the tridentate cavity for Ln^{III}, but 1 : 1 [Ln(**L*i***)]$^{3+}$ and 1 : 2 [Ln(**L*i***)$_2$]$^{3+}$complexes can be obtained at submilimolar concentrations in acetonitrile for the three ligands. Obviously, the triple-helical complexes [Ln(**L*i***)$_3$]$^{3+}$ are more sensitive to steric effects because of the location of a large number of terminal amide groups along the three-fold axis. The associated cumulative formation constants are thus reduced by 3–4 orders of magnitude when going from [Ln(**L5**)$_3$]$^{3+}$ to [Ln(**L6**)$_3$]$^{3+}$, and they become too small to be determined for [Ln(**L7**)$_3$]$^{3+}$ which eventually establishes that peripheral interstrand interactions can control the wrapping process, a crucial point for generating size-discriminating effects.[3,6] However, no peak of selectivity is evidenced along the lanthanide series for [Ln(**L*i***)$_3$]$^{3+}$ (*i* = 5, 6) which strongly constrasts with related steric effects in [Ln(**L4**)$_3$]$^{3+}$ favoring the complexation of mide-range Ln^{III}.[15] This difference can be traced back to the extreme rigidity of the helically wrapped strands in the latter complexes producing interstrand dispersive (*i.e.* π-stacking) forces which optimizes the cavity for a precise ionic radius. For [Ln(**L*i***)$_3$]$^{3+}$ (*i* = 5, 6), the larger flexibility provided by the carboxamide side arms limits size-discrimination, which translates into a simple inversion of the classical electrostatic trends when going from **L5** to **L6**. As far as 1 : 2 complexes [Ln(**L6**)$_2$(H$_2$O)$_2$(CF$_3$SO$_3$)]$^{2+}$ and [Ln(**L7**)$_2$(H$_2$O)$_2$(CF$_3$SO$_3$)]$^{2+}$ are concerned, we observe very

Table 6 Selected bond lengths (Å) and bond angles (°) in $[Tb(\mathbf{L8})_3]_2(CF_3SO_3)_6(CH_3CH_2CN)_3(H_2O)$ (**11**)

	Tb1, **11a**			Tb2, **11b**		
	Strand a	Strand b	Strand c	Strand d	Strand e	Strand f
Bond lengths						
Tb–O1	2.356(8)	2.386(9)	2.383(8)	2.387(8)	2.382(8)	2.413(9)
Tb–N1	2.54(1)	2.54(1)	2.54(1)	2.51(1)	2.49(1)	2.51(1)
Tb–O2	2.365(9)	2.405(9)	2.331(7)	2.396(9)	2.411(9)	2.415(9)
Bite angles						
Tb1, **11a**				Tb2, **11b**		
N–Ln–N						
N1a–Tb1–N1b	120.1(3)			N1d–Tb2–N1e	119.2(4)	
N1a–Tb1–N1c	123.0(3)			N1e–Tb2–N1f	120.4(3)	
N1b–Tb1–N1c	116.9(3)			N1f–Tb2–N1d	120.4(4)	
O–Ln–N						
O1a–Tb1–N1b	72.7(3)			O1d–Tb2–N1e	139.1(3)	
O2a–Tb1–N1b	139.7(3)			O2d–Tb2–N1e	71.1(3)	
O1a–Tb1–N1c	138.6(3)			O1d–Tb2–N1f	71.6(3)	
O2a–Tb1–N1c	71.9(3)			O2e–Tb2–N1f	134.9(3)	
O1b–Tb1–N1a	139.4(3)			O1e–Tb2–N1d	138.3(3)	
O2b–Tb1–N1a	73.1(3)			O2e–Tb2–N1d	74.1(3)	
O1b–Tb1–N1c	70.1(3)			O1e–Tb2–N1f	72.1(3)	
O2b–Tb1–N1c	134.9(3)			O2e–Tb2–N1f	134.9(3)	
O1c–Tb1–N1a	73.4(4)			O1f–Tb2–N1d	74.6(3)	
O2c–Tb1–N1a	137.9(3)			O2f–Tb2–N1d	134.3(3)	
O1c–Tb1–N1b	140.3(3)			O1f–Tb2–N1e	133.9(3)	
O2c–Tb1–N1b	69.5(3)			O2f–Tb2–N1e	76.8(3)	
O–Ln–O						
O1a–Tb1–O1b	81.3(3)			O1d–Tb2–O1e	143.7(3)	
O1a–Tb1–O1c	83.1(3)			O1d–Tb2–O1f	87.0(3)	
O1a–Tb1–O2b	86.3(3)			O1d–Tb2–O2e	80.4(3)	
O1a–Tb1–O2c	142.2(3)			O1d–Tb2–O2f	76.5(3)	
O2a–Tb1–O1b	142.0(4)			O2d–Tb2–O1e	81.6(3)	
O2a–Tb1–O1c	79.9(3)			O2d–Tb2–O1f	79.6(3)	
O2a–Tb1–O2b	82.1(3)			O2d–Tb2–O2e	85.6(3)	
O2a–Tb1–O2c	82.7(3)			O2d–Tb2–O2f	147.7(3)	
O1b–Tb1–O1c	81.9(3)			O1e–Tb2–O1f	77.2(3)	
O1b–Tb1–O2c	82.7(3)			O1e–Tb2–O2f	87.4(3)	
O2b–Tb1–O1c	146.2(3)			O2e–Tb2–O1f	148.7(3)	
O2b–Tb1–O2c	77.2(3)			O2e–Tb2–O2f	77.3(3)	

similar structural and photophysical behaviours which point to negligible electronic coupling between the terminal alkyl or aryl groups and the tridentate bis-carboxamidopyridine core. Two noticeable differences merit to be mentioned. (1) A slightly improved **L7** $\longrightarrow$ Ln^{III} (Ln = Eu, Tb) energy transfer process increases quantum yields in solution for complexes with **L7**, but the light-conversion process remains modest because of the global inefficient ligand-centered sensitization. (2) The dynamic of solvent exchange in the first coordination sphere is faster for $[Ln(\mathbf{L7})_2(H_2O)_2(CF_3SO_3)]^{2+}$, thus leading to an average C_{2h} or D_2 symmetry on the NMR time scale while $[Ln(\mathbf{L6})_2(H_2O)_2(CF_3SO_3)]^{2+}$ exhibits C_2 symmetry. Some hydrophobic effects resulting from the four benzyl groups may be invoked for rationalizing a restricted access of the first coordination sphere together with weaker interactions with solvent molecules in $[Ln(\mathbf{L7})_2(H_2O)_2(CF_3SO_3)]^{2+}$. Finally, the connection of a single benzyl groups to each amide side arm in **L8** restores the formation of stable triple-helical complexes $[Ln(\mathbf{L8})_3]^{3+}$, but the blocked rotations round the OC–N bonds produce intricate mixtures of inert conformers in solution which strongly limit the characterization process.

Since closely related carboxamido-pyridine binding units are used in extended triple-helical polymetallic d–f[38] and f–f[39] helicates and in sophisticated nine-coordinated podates,[35,40] we can now foresee that (i) improved light-harvesting properties in related complexes can be only envisioned with the introduction of a single substituted benzyl groups absorbing in the near-UV per carboxamide side arms and (ii) significant size-discrimination along the the lanthanide series cannot rely on simple steric crowding along the three-fold axis. These two points are crucial for the design of segmental ligands programmed for the selective preparation of pure heterometallic f–f helicates.[6,41] Obviously, neutral 2,6-dicarboxamidopyridine ligands provide too small entropic contributions upon complexation with Ln(III) to provide stable asssemblies in water, and the complexes described here are to be modified if their use as sensors in biological media is foresee. However, the recent combination of one amide and one carboxylate side arms connected at the 2 and 6 positions of the central pyridine ring in nine-coordinate podands demonstrates that the design of related water-stable complexes is within reach.[35]

Experimental

Solvents and starting materials

These were purchased from Fluka AG (Buchs, Switzerland) and used without further purification unless otherwise stated. Thionyl chloride was distilled from elemental sulfur, acetonitrile, dichloromethane, *N*,*N*-dimethylformamide were distilled from CaH_2. Silicagel (Acros, 0.035–0.07 mm) was used for preparative column chromatography. The triflate salts $Ln(CF_3SO_3)_3 \cdot xH_2O$ (Ln = La–Lu) were prepared from the corresponding oxides (Rhodia, 99.99%) and dried according to published procedures.[42] The Ln content of solid salts was determined by complexometric titrations with Titriplex III (Merck) in the presence of urotropine and xylene orange.[43]

Preparation of *N*,*N*,*N*′,*N*′-tetraalkylpyridine-2,6-dicarboxamide (R = isopropyl: L6, R = benzyl: L7), and *N*,*N*′-dibenzylpyridine-2,6-dicarboxamide (L8)

2,6-Dipicolinic acid (3.06 g, 18.3 mmol) was refluxed with thionyl chloride (40 cm^3, 550 mmol) and *N*,*N*-dimethylformamide (0.1 cm^3) for 1 h. Excess thionyl chloride was evaporated and the crude residue co-evaporated with dichloromethane (10 cm^3). The dried solid residue was dissolved in dichloromethane (25 cm^3) at 0 °C, and *N*,*N*-dialkylamine (183 mmol, alkyl = isopropyl: **L6**, alkyl = benzyl: **L7**),) or *N*-benzylamine (183 mmol, **L8**) was added dropwise under an inert N_2 atmosphere. The resulting solution was refluxed for 1 h and evaporated. The yellow residue was partitioned between dichloromethane (200 cm^3) and aq. NaOH (0.01 M, 150 cm^3). The organic phase was washed with water (2 × 100 cm^3), dried (Na_2SO_4) and evaporated to dryness. The resulting crude compound was purified by column chromatography (silica gel, CH_2Cl_2–MeOH 99 : 1) and crystallized in CH_2Cl_2–diethyl ether (**L6** and **L7**) or acetonitrile (**L8**) to afford **L6**, **L7** and **L8** as white solids (80–82% yields).

L6: Mp = 167 °C. ^{1}H NMR (d^6-DMSO): δ 1.05 (CH_3, d, J^3 = 7 Hz, 12H), 1.39 (CH_3, d, J^3 = 7 Hz, 12H), 3.55 (CH, hept, J^3 = 7 Hz, 2H), 3.56 (CH, hept, J^3 = 7 Hz, 2H), 7.39 (H2, d, J^3 = 7.5 Hz, 2H), 7.91 (H1, t, J^3 = 7.5 Hz, 1H). ESI-MS (CH_2Cl_2–CH_3OH = 9 : 1): *m*/*z* 356.3 ($[M + Na]^+$). Anal. Calc. for $C_{19}H_{31}N_3O_2$: C, 68.43; N, 12.60; H, 9.37. Found: C, 67.8; N, 12.4; H, 9.4%.

L7: Mp = 90 °C. ^{1}H NMR (d^6-DMSO): δ 4.26 (CH_2, s, 4H), 4.49 (CH_2, s, 4H), 7.06–7.34 (CH-aryl, m, 20H), 7.69 (H2, d, J^3 = 8 Hz, 2H), 8.00 (H1, t, J^3 = 8 Hz, 1H). ESI-MS (CH_2Cl_2–CH_3OH = 9 : 1): *m*/*z* 548.3 ($[M + Na]^+$). Anal. Calc. for $C_{35}H_{31}N_3O_2$: C, 79.9; N, 7.99; H, 5.94. Found: C, 80.3; N, 7.8; H, 6.1%.

L8: Mp = 180 °C. ^{1}H NMR (d^6-DMSO): δ 4.56 (CH_2, d, J^3 = 6 Hz, 4H), 7.16–7.29 (CH-aryl, m, 10H), 8.12–8.23 (H1–H2, AB_2, J^3 = 8 Hz, 3H), 9.86 (NH, t, J^3 = 6 Hz, 1H). ESI-MS (CH_2Cl_2–CH_3OH = 9 : 1): *m*/*z* 368.2 ($[M + Na]^+$). Anal. Calc. for $C_{21}H_{19}N_3O_2$: C, 73.02; N, 12.17; H, 5.54. Found: C, 72.7; N, 12.0; H, 5.5%.

Preparation of the complexes $[Ln(L6)_2](CF_3SO_3)_3 \cdot xH_2O \cdot yTHF$ (Ln = Eu, *x* = 2, *y* = 0: 1; Ln = Gd, *x* = *y* = 0: 2; Ln = Tb, *x* = *y* = 0: 3; Ln = Lu, *x* = 0, *y* = 1.5: 4) and $[Ln(L7)_2](CF_3SO_3)_3 \cdot xH_2O \cdot yTHF$ (Ln = Eu, *x* = 1, *y* = 0: 5; Ln = Gd, *x* = 0, *y* = 2: 6; Ln = Tb, *x* =3, *y* = 0: 7; Ln = Lu, *x* = 1, *y* = 0: 8)

A solution of $Ln(CF_3SO_3)_3 \cdot xH_2O$ (Ln = Eu, Gd, Tb, Lu; 0.017 mmol) in acetonitrile (3 cm^3) was added to a solution of **L6** or **L7** (0.034 mmol) in acetonitrile (3 cm^3). After stirring for 2 h. at RT, acetonitrile was evaporated and the solid residue dissolved in tetrahydrofuran. Diethyl ether was diffused into the solution for 1 day and the resulting white microcrystalline powders were collected by filtration and dried to give 74–84% of $[Ln(L6)_2](CF_3SO_3)_3 \cdot xH_2O \cdot yTHF$ (Ln = Eu, *x* = 2, *y* = 0: **1**; Ln = Gd, *x* = *y* = 0: **2;** Ln = Tb, *x* = *y* = 0: **3;** Ln = Lu, *x* = 0, *y* = 1.5: **4**) and $[Ln(L7)_2](CF_3SO_3)_3 \cdot xH_2O \cdot yTHF$ (Ln = Eu, *x* = 1, *y* = 0: **5**; Ln = Gd, *x* = 0, *y* = 2: **6**; Ln = Tb, *x* =3, *y* = 0: **7**; Ln = Lu, *x* = 1, *y* = 0: **8**). All the complexes were characterized by their IR spectra and gave satisfying analyses (Table S2, ESI) Fragile solvated monocrystals suitable for X-ray diffraction studies have been obtained for $[Eu(L6)_2(H_2O)_2(CF_3SO_3)](CF_3SO_3)_2(THF)_{1.5}$ (**9**) and $[Gd(L7)_2(H_2O)_2(CF_3SO_3)](CF_3SO_3)_2(^tBuOMe)_2$ (**10**) upon ultra slow diffusion of dialkyl ether (diisopropyl for **9** and *tert*-butyl methyl ether for **10**) into a concentrated solution of **1** in THF, and **6** in propionitrile.

Preparation of the complex $[Tb(L8)_3]_2(CF_3SO_3)_6(CH_3CH_2CN)_3(H_2O)$ (11)

A solution of $Tb(CF_3SO_3)_3 \cdot 3H_2O$ (50 mg, 0.076 mmol) in propionitrile (3 cm^3) was added to a solution of **L8** (78 mg, 0.23 mmol) in propionitrile (3 cm^3). After stirring for 3 d. at RT, light petroleum (bp = 40–60 °C) was slowly diffused and the resulting white crystals $[Tb(L8)_3]_2(CF_3SO_3)_6(CH_3CH_2CN)_3(H_2O)$ (**11**) were directly transferred onto the diffractometer. A parallel synthesis with $Eu(CF_3SO_3)_3 \cdot 3H_2O$ provided a microcrystalline powder which was collected by filtration and dried to give 80% of $[Eu(L8)_3](CF_3SO_3)_3$. Anal. Calc. for $Eu(C_{21}H_{19}N_3O_2)_3(CF_3SO_3)_3$: C, 48.47; N, 7.71; H, 3.51. Found: C, 48.1; N, 7.6; H, 3.6%.

Crystal structure determinations of L8, $[Eu(L6)_2(H_2O)_2(CF_3SO_3)](CF_3SO_3)_2(THF)_{1.5}$ (9), $[Gd(L7)_2(H_2O)_2(CF_3SO_3)](CF_3SO_3)_2(^tBuOMe)_2$ (10) and $[Tb(L8)_3]_2(CF_3SO_3)_6(CH_3CH_2CN)_3(H_2O)$ (11)

A summary of crystal data, intensity measurements and structure refinement are collected in Table 7. All crystals were mounted on quartz fibre with protection oil. Cell dimensions and intensities were measured at 200 K on a Stoe IPDS diffractometer with graphite-monochromated Mo-Kα radiation (λ = 0.71073 Å). Data were corrected for Lorentz and polarization effects and for absorption. The structure were solved by direct methods (SIR97),[44] all other calculation were performed with XTAL[45] system and ORTEP[46] programs.

L8. The hydrogen atoms were observed and refined with fixed isotropic parameters (0.05 Å^2). CCDC reference number 213297.

$[Eu(L6)_2(H_2O)_2(CF_3SO_3)](CF_3SO_3)_2(THF)_{1.5}$ (**9**). The hydrogen atoms of the two water molecules were observed and refined with fixed isotropic parameters (0.05 Å^2). One of the THF molecule was refined with a population parameter of 0.5. CCDC reference number 213298

$[Gd(L7)_2(H_2O)_2(CF_3SO_3)](CF_3SO_3)_2(^tBuOMe)_2$ (**10**). The benzyl group C29b–C35b was disordered and refined on two positions with population parameters of 0.5 (C30b was common to both positions). The phenyl C23b–C28b was also disordered and showed large anisotropic displacement parameters in the mean plane of the aromatic ring. Refinement on a set of specific positions did not provide satisfying results and this suggested the existence of a dynamic disorder producing statistical positions. The ^{t}BuOMe group g was disordered and refined with restraints on bond distances and bond angles on two positions possessing a common position for C5g with population parameters of 0.6 and 0.4. The minor site g′ was refined with isotropic displacement parameters. CCDC reference number 213299.

$[Tb(L8)_3]_2(CF_3SO_3)_6(CH_3CH_2CN)_3(H_2O)$ (**11**). The complex crystallized in the polar space group $P2_1$ and exhibited pairs of domain structures twinned by inversion in variables ratios for each crystal. The refinement of the Flack parameter[47] showed reliable values of the inversion-distinguishing power:[48] *x* = 0.07(1) for the selected crystal, unambigously showing that the crystal structure was non-centrosymmetric with an inversion twin ratio of 0.93 : 0.07 (Fig. S8, ESI †). The propionitrile

Table 7 Summary of crystal data for **L8**, $[Eu(\mathbf{L6})_2(H_2O)_2(CF_3SO_3)](CF_3SO_3)_2(THF)_{1.5}$ (**9**), $[Gd(\mathbf{L7})_2(H_2O)_2(CF_3SO_3)](CF_3SO_3)_2(^tBuOMe)_2$ (**10**) and $[Tb(\mathbf{L8})_3]_2(CF_3SO_3)_6(CH_3CH_2CN)_3(H_2O)$ (**11**)

	L8	**9**	**10**	**11**
Formula	$C_{21}H_{19}N_3O_2$	$C_{47}H_{78}EuF_9N_6O_{16.5}S_3$	$C_{83}H_{90}F_9GdN_6O_{17}S_3$	$C_{141}H_{131}F_{18}N_{21}O_{31}S_6Tb_2$
M_r	345.4	1410.5	1868.2	3468.1
Crystal system	Monoclinic	Monoclinic	Monoclinic	Monoclinic
Space group	$P2_1/c$	$P2_1/c$	$I2/a$	$P2_1$
a/Å	15.9562(12)	14.6845(6)	24.0530(11)	16.0103(7)
b/Å	11.0886(8)	25.3495(13)	15.0320(6)	28.0794(13)
c/Å	9.9212(7)	18.3302(8)	48.983(3)	17.3614(7)
β/°	97.695(9)	101.303(5)	99.378(6)	93.889(5)
U/Å^3	1739.6(2)	6691.0(6)	17473.8(15)	7787.0(6)
Z	4	4	8	2 ($Z' = 2$)
D_c/g cm^{-3}	1.319	1.400	1.420	1.479
μ(Mo-Kα) mm^{-1}	0.087	1.118	0.917	1.080
No. measured reflc.	18736	65007	116662	68845
No. unique reflc.	3365	12398	20939	30394
No. observed reflc.	1564	8091	11243	21740
Flack parameter x	–	–	–	0.069(12)
R, wR	0.031, 0.031	0.033, 0.035	0.037, 0.037	0.041, 0.042

molecules were refined with isotropic displacement parameters. The fluorine atoms of triflates k and l were disordered and refined with isotropic displacement parameters, and restraints on bond distances and bond angles. CCDC reference number 213300.

See http://www.rsc.org/suppdata/dt/b3/b307413g/ for crystallographic data in CIF or other electronic format.

Spectroscopic and analytical measurements

Electronic spectra in the UV-Vis were recorded at 20 °C from solutions in MeCN with a Perkin-Elmer Lambda 900 spectrometer using quartz cells of 0.1 and 1 mm path length. Spectrophotometric titrations were performed with a J&M diode array spectrometer (Tidas series) connected to an external computer. In a typical experiment, 50 cm^3 of **L6** in acetonitrile (10^{-4} mol dm^{-3}) were titrated at 20 °C with a solution of $Ln(CF_3SO_3)_3 \cdot xH_2O$ (10^{-3} mol dm^{-3}) in acetonitrile under an inert atmosphere. After each addition of 0.10 ml, the absorbences were recorded using Hellma optrodes (optical path length 0.1 cm) immersed in the thermostated titration vessel and connected to the spectrometer. Mathematical treatment of the spectrophotometric titrations was performed with factor analysis[25] and with the SPECFIT program.[26] IR spectra were obtained from KBr pellets with a Perkin Elmer 883 spectrometer. ^{1}H and ^{13}C NMR spectra were recorded at 25 °C on a Broadband Varian Gemini 300 spectrometer. Chemical shifts are given in ppm with respect to TMS. Pneumatically-assisted electrospray (ESI-MS) mass spectra were recorded from 10^{-4} mol dm^{-3} acetonitrile solutions on a Finnigan SSQ7000 instrument. Excitation and emission spectra as well as lifetime measurements were recorded on a Perkin-Elmer LS-50B spectrometer equipped for low-temperature measurements. The quantum yields Φ have been calculated using the equation

$$\frac{\Phi_x}{\Phi_r} = \frac{A_r(\tilde{\nu})I_r(\tilde{\nu})n_x^2D_x}{A_x(\tilde{\nu})I_x(\tilde{\nu})n_r^2D_r},$$

where x refers to the sample and r to the reference; A is the absorbance, $\tilde{\nu}$ the excitation wavenumber used, I the intensity of the excitation light at this energy, n the refractive index and D the integrated emitted intensity.[33] $[Eu(terpy)_3](ClO_4)_3$ (Φ_{tot}^{Eu} = 1.3%, acetonitrile, 10^{-3} mol dm^{-3}) and $[Tb(terpy)_3](ClO_4)_3$ (Φ_{tot}^{Tb} = 4.7%, acetonitrile, 10^{-3} mol dm^{-3}) were used as references for the determination of quantum yields of the Eu- and Tb-containing samples, respectively.[16,40] Elemental analyses were performed by Dr H. Eder from the microchemical Laboratory of the University of Geneva.

Acknowledgements

This work is supported through grants from the Swiss National Science Foundation. We thank Hélène Lartigue and Bernard Bocquet for technical support.

References

1 N. Kaltsoyannis and P. Scott, *The f-Elements*, Oxford University Press, Oxford, 1999.

2 For recent reviews, see: (*a*) C. Görller-Walrand and K. Binnemans, in *Handbook on the Physics, and Chemistry of Rare Earths*, ed. K. A. Gschneidner and L. Eyring, North-Holland Publishing Company, Amsterdam, 1996, vol. 23, pp. 121–283; (*b*) P. Porcher, in *Rare Earths*, ed. R. Saez Puche and P. Caro, Editorial Complutense S.A., Madrid, 1998, pp. 43–66; (*c*) C. Görller-Walrand and K. Binnemans, in *Handbook on the Physics, and Chemistry of Rare Earths*, ed. K. A. Gschneidner and L. Eyring, North-Holland Publishing Company, Amsterdam, 1998, vol. 25, pp. 101–264; (*d*) C. Piguet and C. F. C. G. Geraldes, in *Hanbook on the Physics, and Chemistry of Rare Earths*, ed. K. A. Gschneidner, J.-C. G. Bünzli and V. Pecharsky, North-Holland Publishing Company, Amsterdam, 2003, vol. 33, ch. 215, pp. 353–463.

3 C. Piguet and J.-C. G. Bünzli, *Chem. Soc. Rev.*, 1999, **28**, 347.

4 (*a*) F. Berny, N. Muzet, L. Troxler, A. Dedieu and G. Wipff, *Inorg. Chem.*, 1999, **38**, 1244; (*b*) M. Baaden, F. Berny, C. Madic and G. Wipff, *J. Phys. Chem. A.*, 2000, **104**, 7659; (*c*) C. Rabbe, V. Mikhalko and J.-P. Dognon, *Theor. Chem. Acc.*, 2000, **104**, 280; (*d*) G. Wipff and F. Berny, *J. Chem. Soc., Perkin Trans. 2*, 2001, 73.

5 (*a*) G. R. Choppin, in *Lanthanide Probes in Life, Chemical, and Earth Sciences*, ed. J.-C. G. Bünzli and G. R. Choppin, Elsevier, Amsterdam, 1989, ch. 1; (*b*) G. Ionova, C. Rabbe, R. Guillaumont, S. Ionov, C. Madic, J.-C. Krupa and D. Guillaneux, *New J. Chem.*, 2002, **26**, 234.

6 J.-C. G. Bünzli and C. Piguet, *Chem. Rev.*, 2002, **102**, 1897.

7 (*a*) D. A. Durham, G. H. Frost and F. A. Hart, *J. Inorg. Nucl. Chem.*, 1969, **31**, 833; (*b*) R. D. Chapman, R. T. Loda, J. P. Riehl and R. W. Schwartz, *Inorg. Chem.*, 1984, **23**, 1652.

8 C. Mallet, R. P. Thummel and C. Hery, *Inorg. Chim. Acta*, 1993, **210**, 223.

9 (*a*) L. I. Semenova, A. N. Sobolev, B. W. Skelton, and A. H. White, *Aust. J. Chem.*, 1999, **52**, 519; (*b*) G. Muller, J.-C. G. Bünzli, J. P. Riehl, D. Suhr, A. von Zelewsky and H. Mürner, *Chem. Commun.*, 2002, 1522.

10 H.-R. Mürner, E. Chassat, R. P. Thummel and J.-C. G. Bünzli, *J. Chem. Soc., Dalton Trans.*, 2000, 2809.

11 J.-C. Berthet, Y. Miquel, P. B. Iveson, M. Nierlich, P. Thuery, C. Madic and M. Ephritikhine, *J. Chem. Soc., Dalton Trans.*, 2002, 3265.

12 (*a*) S. Colette, B. Amekraz, C. Madic, L. Berthon, G. Cote and C. Moulin, *Inorg. Chem.*, 2002, **41**, 7031; (*b*) S. Colette, B. Amekraz, C. Madic, L. Berthon, G. Cote and C. Moulin, *Inorg. Chem.*, 2003, **42**, 2215.

13 M. J. Hudson, M. G. B. Drew, M. R. S. Foreman, C. Hill, N. Huet, C. Madic and T. G. A. Youngs, *Dalton Trans.*, 2003, 1675.
14 D. A. Bardwell, J. C. Jeffery, P. L. Jones, J. A. McCleverty, E. Psillakis, Z. Reeves and M. D. Ward, *J. Chem. Soc., Dalton Trans.*, 1997, 2079.
15 (*a*) C. Piguet, J.-C. G. Bünzli, G. Bernardinelli and A. F. Williams, *Inorg. Chem.*, 1993, **32**, 4139; (*b*) C. Piguet, J.-C. G. Bünzli, G. Bernardinelli, C. G. Bochet and P. Froidevaux, *J. Chem. Soc., Dalton Trans.*, 1995, 83; (*c*) S. Petoud, J.-C. G. Bünzli, F. Renaud, C. Piguet, K. J. Schenk, and G. Hopfgartner, *Inorg. Chem.*, 1997, **36**, 5750.
16 S. Petoud, J.-C. G. Bünzli, C. Piguet, Q. Xiang and R. Thummel, *J. Luminesc.*, 1999, **82**, 69.
17 (*a*) H. Nozary, C. Piguet, P. Tissot, G. Bernardinelli, J.-C. G. Bünzli, R. Deschenaux and D. Guillon, *J. Am. Chem. Soc.*, 1998, **120**, 12274; (*b*) H. Nozary, C. Piguet, J.-P. Rivera, P. Tissot, P.-Y. Morgantini, J. Weber, G. Bernardinelli, J.-C. G. Bünzli, R. Deschenaux, B. Donnio and D. Guillon, *Chem. Mater.*, 2002, **14**, 1075; (*c*) C. Piguet, A. F. Williams, G. Bernardinelli, E. Moret and J.-C. G. Bünzli, *Helv. Chim. Acta*, 1992, **75**, 1697.
18 (*a*) G. Zucchi, R. Scopelliti and J.-C. G. Bünzli, *J. Chem. Soc., Dalton Trans.*, 2001, 1975; (*b*) A. Beeby, L. M. Bushby, D. Maffeo and J. A. G. Williams, *J. Chem. Soc., Dalton Trans.*, 2002, 48; (*c*) G. Zucchi, A.-C. Ferrand, R. Scopelliti and J.-C. G. Bünzli, *Inorg. Chem.*, 2002, **41**, 2459; (*d*) A. Dadabhoy, S. Faulkner and P. G. Sammes, *J. Chem. Soc., Perkin Trans. 2*, 2002, 348.
19 F. Renaud, C. Piguet, G. Bernardinelli, J.-C. G. Bünzli and G. Hopfgartner, *Chem. Eur. J.*, 1997, **3**, 1646.
20 M. Pons and O. Millet, *Prog. Nucl. Magn. Reson. Spectrosc.*, 2001, **38**, 267.
21 H. Günther, *Spectroscopy*, John Wiley & Sons, Chichester–New York–Brisbane–Toronto, 1980, p. 244.
22 M. C. Etter, *J. Phys. Chem.*, 1991, **95**, 4601.
23 J. F. Malone, C. M. Murray, G. M. Dolan, R. Docherty and A. J. Lavery, *Chem. Mater.*, 1997, **9**, 2983.
24 F. H. Allen, O. Kennard, D. G. Watson, L. Brammer, A. G. Orpen and R. Taylor, *J. Chem. Soc., Perkin Trans. 2*, 1987, S1.
25 E. R. Malinowski and D. G. Howery, *Factor Analysis in Chemistry*, Wiley, New York–Chichester, 1980.
26 (*a*) H. Gampp, M. Maeder, C. J. Meyer and A. D. Zuberbühler, *Talanta*, 1986, **33**, 943; (*b*) H. Gampp, M. Maeder, C. J. Meyer and A. D. Zuberbühler, *Talanta*, 1985, **23**, 1133.
27 (*a*) G. Hopfgartner, C. Piguet and J. D. Henion, *J. Am. Soc. Mass Spectrom.*, 1994, **5**, 748; (*b*) E. Leize, A. Jaffrezic and A. van Dorsselaer, *J. Mass Spectrom.*, 1996, **31**, 537; (*c*) C. A. Schalley, *Int. J. Mass Spectrom.*, 2000, **194**, 11.
28 N. Ouali, B. Bocquet, S. Rigault, P.-Y. Morgantini, J. Weber and C. Piguet, *Inorg. Chem.*, 2002, **41**, 1436.
29 R. D. Shannon, *Acta. Crystallogr., Sect. A*, 1976, **32**, 751.
30 A. G. Orpen, L. Brammer, F. H. Allen, O. Kennard, D. G. Watson and R. Taylor, *J. Chem. Soc., Dalton Trans.*, 1989, S1.
31 J.-C. G. Bünzli, B. Klein, G. Chapuis and K. J. Schenk, *Inorg. Chem.*, 1982, **21**, 808.
32 H.-H. Perkampus, *UV-VIS Atals of Organic Compounds*, VCH, Weinheim, 2nd edn., part 2, 1992, p. 338.
33 M. H. V. Werts, R. T. F. Jukes and J. W. Verhoeven, *Phys. Chem. Chem. Phys.*, 2002, **4**, 1542.
34 F. J. Steemers, W. Verboom, D. N. Reinhoudt, E. B. Vandertol and J. W. Verhoeven, *J. Am. Chem. Soc.*, 1995, **117**, 9408.
35 J.-M. Senegas, G. Bernardinelli, D. Imbert, J.-C. G. Bünzli, P.-Y. Morgantini, J. Weber and C. Piguet, *Inorg. Chem.*, 2003, **42**, 4680.
36 (*a*) S. Tobita, M. Arakawa and I. Tanaka, *J. Phys. Chem.*, 1984, **88**, 2697; (*b*) S. Tobita, M. Arakawa and I. Tanaka, *J. Phys. Chem.*, 1985, **89**, 5649.
37 (*a*) N. Sabbatini, M. Guardigli and J.-M. Lehn, *Coord. Chem. Rev.*, 1993, **123**, 201; (*b*) N. Sabbatini, M. Guardigli and I. Manet, in *Handbook on the Physics, and Chemistry of Rare Earths*, ed. K. A. Gschneidner and L. Eyring, Elsevier, Amsterdam, 1996, vol. 23, pp. 69–119; (*c*) F. R. Gonçalves e Silva, O. L. Malta, C. Reinhard, H. U. Güdel, C. Piguet, J. E. Moser and J.-C. G. Bünzli, *J. Phys. Chem. A*, 2002, **106**, 1670.
38 M. Cantuel, G. Bernardinelli, D. Imbert, J.-C. G. Bünzli, G. Hopfgartner and C. Piguet, *J. Chem. Soc., Dalton Trans.*, 2002, 1929, and references therein.
39 S. Floquet, N. Ouali, B. Bocquet, G. Bernardinelli, D. Imbert, J.-C. G. Bünzli, G. Hopfgartner and C. Piguet, *Chem. Eur. J.*, 2003, **9**, 1860, and references therein.
40 F. Renaud, C. Piguet, G. Bernardinelli, J.-C. G. Bünzli and G. Hopfgartner, *J. Am. Chem. Soc.*, 1999, **121**, 9326.
41 N. André, R. Scopelliti, G. Hopfgartner, C. Piguet and J.-C. G. Bünzli, *Chem. Commun.*, 2002, 214.
42 J. F. Desreux, in *Lanthanide Probes in Life, Chemical, and Earth Sciences*, ed. J.-C. G. Bünzli and G. R. Choppin, Elsevier, Amsterdam, 1989, ch. 2, p. 43.
43 G. Schwarzenbach, *Complexometric Titrations*; Chapman & Hall, London, 1957, p. 8.
44 A. Altomare, M. C. Burla, M. Camalli, G. Cascarano, C. Giacovazzo, A. Guagliardi, A. G. G. Moliterni, G. Polidori and R. Spagna, *J. Appl. Crystallogr.*, 1999, **32**, 115.
45 XTAL 3.2 User's Manual, S. R. Hall, H. D. Flack and J. M. Stewart, Eds. Universities of Western Australia and Maryland, 1989.
46 C. K. Johnson, ORTEP II; Report ORNL-5138, Oak Ridge National Laboratory: Oak Ridge, TN, 1976.
47 H. D. Flack and G. Bernardinelli, *Acta. Crystallogr., Sect. A*, 1999, **55**, 908.
48 H. D. Flack and G. Bernardinelli, *J. Appl. Crystallogr.*, 2000, **33**, 1143.